On the Mechanism of Light Harvesting in Photosynthetic Purple Bacteria: B800 to B850 Energy Transfer

Gregory D. Scholes and Graham R. Fleming*

Department of Chemistry, University of California, Berkeley, and Physical Biosciences Division, Lawrence Berkeley National Laboratory, Berkeley, California 94720-1460

Received: September 27, 1999; In Final Form: December 15, 1999

The rate of energy transfer from B800 to B850 in the peripheral light harvesting complex LH2 is modeled in detail. A method for determining ensemble average energy transfer rates in complex, coupled multichromophoric systems is reported and is employed to investigate the interplay of electron−phonon coupling (fast fluctuations of the protein) and site energy disorder (slow fluctuations) on the spectral overlap between donor and acceptor, and therefore the energy transfer rate. A series of model calculations for *Rb. sphaeroides* is reported. The disorder is found to have a marked influence on the calculated rate of energy transfer and is responsible for a faster energy transfer time than would occur in its absence and furthermore accounts for the weak temperature dependence observed in experiment. The excitonic nature of the acceptor (albeit dynamically localized) also has impact in terms of how B850 functions as an energy acceptor. These conclusions are further elucidated by calculations of *Rps. acidophila* B800−B850 and a series of reconstituted complexes containing a systematically blue-shifted B800 absorption band. The role of dielectric effects is considered. It is reported that interaction of the B800 and B850 transition densities with the carotenoids has an effect on the B800−B850 electronic couplings.

I. Introduction

Recently, structures of the peripheral antenna (LH2) pigment−protein complex for two species of purple nonsulfur photosynthetic bacteria have been resolved.[1−3] These data reveal that the structure is comprised of units consisting of two transmembrane polypeptides (α and β) and associated pigments, arranged in a highly symmetric ring motif (C_9 symmetry in *Rhodopseudomonas acidophila* strains 10050 and 7050). The antenna consists of two rings of BChl *a* pigments, B800 and B850, and at least one carotenoid, which makes close contact with chromophores from each of these rings, Figure 1. A similar picture of the peripheral antenna is derived from electron microscopy studies of other species.[4,5] This detailed structural information has motivated intensive study into the relationship between the arrangement of chromophores and the mechanism of light harvesting.[6−39]

Light absorbed by the B800 ring is transferred rapidly to the B850 ring on a time scale of 800 fs in *Rps. acidophila* and 650 fs in *Rb. sphaeroides* at room temperature, increasing to just 1.2 ps at 77 K for both *Rps. acidophila* and *Rb. sphaeroides*.[11,18,40−47] Förster theory, however, provides an unsatisfactory estimate of this time scale, and in particular, fails to elucidate the reasons for the remarkable insensitivity to temperature.[37,48−50] Progress toward construction of a fully realistic description of the light harvesting processes has been hampered by lack of knowledge of electronic couplings, electron−phonon coupling, and site energy distributions in antenna complexes. The high-resolution structure of LH2 from *Rps. acidophila* and *Rs. molischianum*, combined with advances in nonlinear spectroscopy and electronic structure calculations allow us to bring together all the relevant data for the LH2 system, and to examine quantitatively the dynamics of light-harvesting. Of particular importance from an experimental perspective has been the development of the three-pulse echo peak shift (3PEPS) technique,[51−54] along with the associated theory.[29,30,55,56] This experiment enables determination of line shape functions (electron−phonon coupling) in complex baths, the inhomogeneous width of the site energy distribution, as well as the energy transfer time scale(s) in a single experiment. This information is particularly salient because, owing to the disparate time scales characteristic of protein fluctuations, long time disorder (inhomogeneity) in the electronic transition frequencies of antenna pigments underlies any ensemble-average measurement. This disorder, in turn, plays a crucial role in dynamic processes.

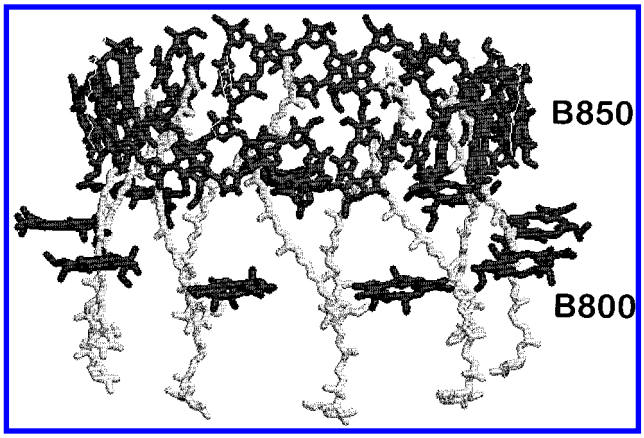

Figure 1. Structure of the LH2 antenna complex (*Rps. acidophila* strain 10050) showing the ring of nine B800 BChls, the 18 B850 BChls, and the nine rhodopin glucoside carotenoids.

In the present report, we address the basis of energy transfer from the B800 ring to the B850 ring in the LH2 complex. We ask the following questions: How can we think about the B850 ring as an energy acceptor? What is the role of disorder,

10.1021/jp993435l CCC: $19.00
Published on Web 02/03/2000

particularly since this characteristic of pigment−protein complexes is fundamentally different to many synthetic light-harvesting systems? We describe a method for incorporating these important details, that is, multichromophoric donor and/or acceptors and static energetic disorder, into a Förster-type energy transfer model. In other words, weak coupling between donor and acceptor is assumed, but no such approximation need be made for couplings withing the donor or acceptor aggregate. In essence, we describe here a more careful, and more illuminating, way of employing Förster theory to calculate rates of energy transfer in complex systems. In this way, we are able to learn quantitatively about the *mechanism* of light harvesting by combining theory and experiment.

We begin by describing our strategy for calculating each constituent of the electronic energy transfer (EET) problem and how we propose to bring these ingredients together, along with experimental input, to calculate ensemble average donor−acceptor spectral overlaps and energy transfer rates. We then report detailed calculations of B800−B850 energy transfer dynamics in *Rb. sphaeroides* from which we draw our primary conclusions regarding the mechanism of EET, and especially the role of disorder. We also examine the impact of the carotenoids that bridge the B800−B850 rings. Finally, the scope of this investigation is extended in section IX, where we report calculations of *Rps. acidophila* strain 10050 wild-type as well as reconstituted complexes that contain various different BChl and Chl molecules in the B800 binding sites. This allows us to delineate further the significance of the B850 band stucture insofar as its role as acceptor density of states in the spectral overlap is concerned.

II. Mechanism of Energy Transfer

The theory of Förster,[57,58] inspired by concentration quenching studies in solution, predicts rates of EET based on the overlap of donor emission and acceptor absorption spectra. This work has been of widespread interest and application; being cited approximately 200 times per year over the past 10 years. Lin later examined this EET process in the context of radiationless transition theory[59] and showed that the electronic coupling factors, V, that control the mechanism, may be separated from the nuclear factors that impart information concerning the temperature dependence, isotope, and energy conservation effects. These nuclear factors are contained in the Förster spectral overlap integral, $J = \int_0^\infty \mathrm{d}\epsilon\, f_D(\epsilon)\, a_A(\epsilon)$. This leads to a flexible formulation for the rate of EET, w, from donor D to acceptor A in terms of area-normalized fluorescence and absorption line shapes, $f_D(\epsilon)$ and $a_A(\epsilon)$ respectively,

$$w = \frac{2\pi}{\hbar}|V|^2 \int_0^\infty \mathrm{d}\epsilon\, f_D(\epsilon)\, a_A(\epsilon) \qquad (1)$$

When significant contributions to the excited electronic states of donor and/or acceptor that are indicative of double excitations from a Hartree−Fock reference determinant in the molecular orbital configuration interaction model can be neglected (i.e., excluding energy transfer involving the polyene or carotenoid 2^1A_g state[60−62]), the electronic coupling that promotes singlet−singlet EET together with dielectric screening effects, D, assumes the form given in eq 2,[63,64]

$$V = (V^{\mathrm{Coul}} + V^{\mathrm{short}})D \qquad (2)$$

where V^{Coul} is the Coulombic interaction between the D* → D and A → A* electronic transition densities,[65,66] which in order to obviate errors arising from the dipole approximation we write as[36−37]

$$V^{\mathrm{Coul}} = \frac{e^2}{4\pi\epsilon_0}\int \mathrm{d}\mathbf{r}_1\, \mathrm{d}\mathbf{r}_2 \frac{P_D(\mathrm{dd}'|\mathbf{r}_1)P_A(\mathrm{a}'\mathrm{a}|\mathbf{r}_2)}{|\mathbf{r}_1 - \mathbf{r}_2|}\Big(\sum_{\mathrm{singles}} 1 - \sum_{\mathrm{doubles}} c_{\mathrm{dd}\to\mathrm{d}'\mathrm{d}'} - \sum_{\mathrm{doubles}} c_{\mathrm{aa}\to\mathrm{a}'\mathrm{a}'}\Big) \qquad (3)$$

where the $P(KL|\mathbf{r}_1)$ are the single particle transition densities[36,37,65] for donor and acceptor molecules. HOMO orbitals are denoted d and a, while LUMO orbitals are primed. In such a description of EET, consideration of the different electron correlation effects in ground and excited states is crucial.[67] Often a CI-singles wave function provides a good description of the excited state, but overestimation of the transition moments results unless CI-doubles contributions are included in the ground state wave function.[68] Thus, we admit explicitly to eq 3 account of double substitutions from the Hartree−Fock reference determinants to the ground state donor and acceptor wave functions via the CI coefficients, c, indicated. In this sense, eq 3 is a generalization of eq 15 in ref 67, to which the reader is referred for a more detailed discussion. In section IIA of that work,[67] it was found that the scaling factor derived from the bracketed terms in eq 3 is approximately 0.65 for the small model dimer examined therein. We conclude that the significance of the CI-doubles contributions of the type suggested by eq 3 are the main reason that the scaling factor needed to be introduced in the "transition density cube" (TDC) method based on CIS transition densities.[37]

The V^{short} contribution to eq 2 encompasses those interactions that are promoted by orbital overlap. Historically one associates such a mechanism with the Dexter exchange integral;[69,70] however, it has been suggested by several authors[71−77] that configuration interaction between locally excited (D*A, DA*) and charge transfer (D^+A^-, D^-A^+) configurations is of considerable importance in mediating this coupling. Indeed, there is strong evidence to suggest that the overwhelming contribution to V^{short} arises from orbital penetration terms that can be interpreted as successive virtual one-electron transfers between donor and acceptor, mediated by the interchromophore ionic configurations.[64,77]

We have determined the B800−B850 electronic couplings using the TDC method, eq 3, as reported previously.[37] We note that, because of the relatively large separations between the B800 and B850 chromophores, these couplings could also be obtained to a reasonable approximation by the dipole approximation, $V^{\mathrm{Coul}} \approx V^{\mathrm{d-d}} = (4\pi\epsilon_0)^{-1}[\vec{\mu}_D\cdot\vec{\mu}_A - 3(\vec{\mu}_D\cdot\hat{R})(\vec{\mu}_A\cdot\hat{R})]/R^3$, with $R = |\mathbf{r}_1 - \mathbf{r}_2|$. However, in the present work, we are particularly interested in elucidating the nature of the B850 acceptor, and hence we need to know details of the couplings within the B850 ring. These couplings must be determined with care because of the close interactions between these molecules (9 Å center-to-center separations and an overlapping pyrrole ring with a face-to-face separation of 3.5 Å). Both Coulombic and overlap dependent contributions should be considered. Calculations of these couplings using a scheme based on ab initio CI-singles/6-31G* wave functions were reported by the present authors recently.[36] To test the integrity of these couplings, we have simulated the absorption and circular dichroism spectra for the B850 ring using these results. We find that the essential features, Figure 2, compare well with experiment.[14,15,19,20] Since these spectra are highly sensitive to the magnitude of the electronic couplings, we conclude that our electronic couplings are reasonably accurate. Note, however,

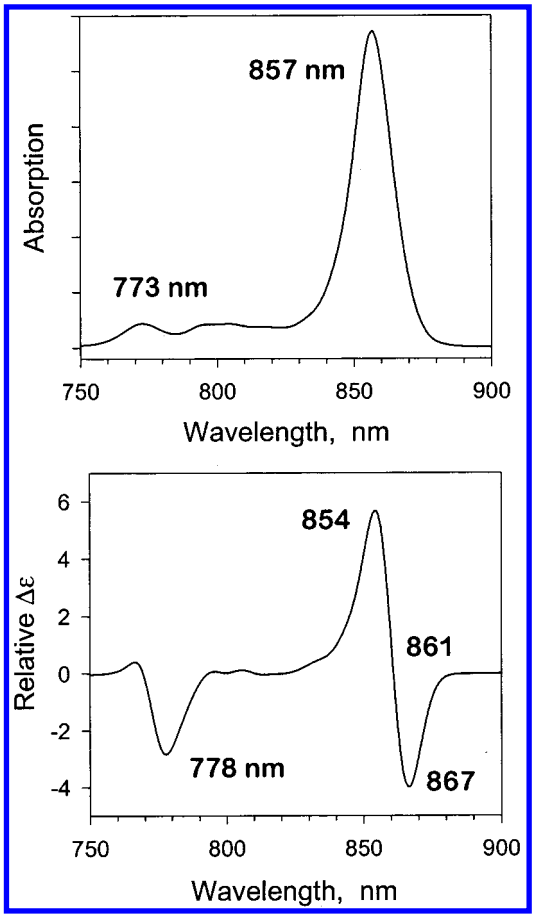

Figure 2. Absorption and CD spectra calculated for the B850 band of *Rb. sphaeroides* at 77 K using the parameters described in the text. Peak positions and the CD zero crossing are indicated.

that in comparison with the experimental data for the B800-deficient mutant reported by Koolhaas et al.[19] the negative peak of the calculated CD signal in the upper exciton region (ca. 780 nm) is too intense relative to the main feature. We return to this point in section VII. The absorption spectrum was calculated using eq 10, described below. The CD spectrum was calculated using an analogous equation, but replacing the transition dipole strength (i.e., $|\mu_\alpha|^2$) with the rotational strength for each exciton level α with excitation energy ϵ_α and corresponding wavelength λ_α (see, e.g., ref 78) determined using eq 4,

$$R(\epsilon_\alpha) = \frac{\pi}{2\lambda_\alpha}\sum_{i,j}\mathbf{R}_{ij}\cdot\langle\alpha|\vec{\mu}_i \times \vec{\mu}_j|0\rangle \qquad (4)$$

where $\mathbf{R}_{ij}$ is the center-to-center separation vector of molecules i and j, which have transition moment vectors $\vec{\mu}_i$ and $\vec{\mu}_j$. The line shapes and disorder used here are those described in section V.

III. Dielectric Screening Effects

The factor D in eq 2 denotes the dielectric screening effects due to the medium in which donor and acceptor are embedded. Typical BChl separations between B800 and B850 are ≥18 Å, and the protein environment constitutes a complex dielectric medium with something of the order of 60 amino acid residues comprising the intervening α and β apoprotein helices,[79] as well as a proximate carotenoid. We consider the effect of the carotenoid in section VII. This environment is depicted in Figure 3.

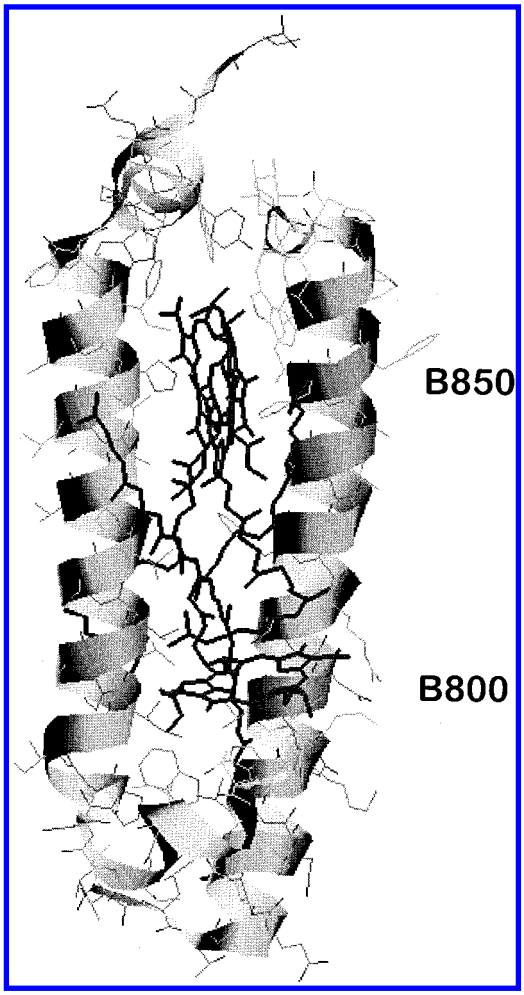

Figure 3. Illustration of the protein environment surrounding the B800−B850 repeat unit. The protein α-helices are highlighted as ribbons.

A case for examining further the possible dielectric screening of the coupling owing to interaction with this environment can be established by considering the Förster equation,[57,58] wherein the coupling is assumed to be modulated by a factor $D = n^{-2}$, where $n = \epsilon_r^{1/2}$ is the refractive index of the medium at optical frequencies. Typically it is assumed that the refractive index of a protein is $n \approx 1.5$, such that the rate of EET is attenuated by a factor of $n^{-4} \approx 0.2$ relative to that in vacuo! This result is obtained if one assumes the dipole approximation for V, that D and A are well separated in a nondispersive, isotropic host medium, and that local field corrections are negligible.[80] Consideration of these approximations and inspection of the complex environment about D and A in Figure 3 leads one to question whether $D = n^{-2}$ is a particularly good assumption. Resolution of this matter is especially vital considering that D can have such a substantive impact on the calculated rate of EET. We note that in some previous studies of energy transfer between rigidly constrained naphthalene and anthracene chromophores, held at a separation of 12 Å by a norbornalogue bridge,[81] and a series of similar bisnaphthalene molecules[82] no significant modulation of the electronic couplings as a function of solvent could be detected. If $D = n^{-2}$ then variations in the bisnaphthalene exciton splittings (of about 5%) between *n*-hexane and acetonitrile solvents should have been observable.

To avoid the first two approximations listed above, one can incorporate screening effects directly into the TDC calculation via eq 5,[80]

$$V^{\mathrm{Coul}} = \frac{e^2}{4\pi\epsilon_0}\int \mathrm{d}\mathbf{r}\,\mathrm{d}\mathbf{r}_1\,\mathrm{d}\mathbf{r}_2 \frac{\mathrm{Re}\,\epsilon_{\mathrm{L}}^{-1}(\mathbf{r},E)\,P_{\mathrm{D}}(\mathrm{dd}'|\mathbf{r}_1)\,P_{\mathrm{A}}(\mathrm{a}'\mathrm{a}|\mathbf{r}_2)}{|\mathbf{r}+\mathbf{r}_1-\mathbf{r}_2|} \quad (5)$$

where the longitudinal dielectric constant can be approximated as $\epsilon_{\mathrm{L}}^{-1}(\mathbf{r},E) = \epsilon^{-1}(E)\,\delta(\boldsymbol{r})$ and the electron correlation terms have been omitted for clarity. This equation accounts for the "volume" in the dielectric medium occupied by D and A, and hence their transition densities, but ignores local field effects.

Craig and Thirunamachandran reported a microscopic theory based on the molecular quantum electrodynamics framework for the influence of the medium on the rate of EET, including each possible interaction from D to A via the medium explicitly.[83] This is reminiscent of a superexchange formalism,[84] and analogously the rate of EET may be either increased or decreased at close D−A separations. However, owing to the substantial excitation energy difference between BChl and amino acid residues, we conclude that this microscopic mechanism is not very significant in the present case. Recently, Juzeliunas and Andrews have reported a detailed many-body description of EET based on the QED formalism[85−87] (explicitly based on the dipole approximation). By considering the energy transfer to be mediated by bath polaritons (medium-dressed photons), this theory accounts for the modification of the bare coupling tensor by screening effects of the medium as well as local field effects. Note that this modification of the coupling is different, in essence, from the refractive index dependence of real photon absorption or emission processes. They obtain the result

$$D = \epsilon_r^{-1}[(\epsilon_r + 2)/3]^2 \quad (6)$$

for large D−A separations (i.e., several molecular diameters). Assuming $n \approx 1.5$ for a membrane protein, then from this equation we estimate $D \approx 0.9$, in other words the rate of EET is attenuated by a factor of approximately 0.8 relative to vacuum.

IV. Ensemble Average Rate of Energy Transfer

To model energy transfer in the LH2 complex, indeed, in pigment−protein complexes in general, we invoke a separation of time scales of the (protein) bath fluctuations such that those motions that induce line-broadening on a more rapid time scale than that for EET (often referred to as the "homogeneous" line-broadening) contribute directly to the calculation of the spectral overlap part of the Förster equation. On the other hand, the fluctuations that are slow compared to the time scale of EET are seen as static disorder ("inhomogeneous" line-broadening) and are accounted for by ensemble averaging. It is the interplay of these two line-broadening mechanisms (time scales) that characterize spectroscopy in pigment−protein complexes,[11,13,30,53,88−97] and as we find in the present work is largely responsible for making natural light-harvesting antennae unique in their function, since such an environment is not characteristic of synthetic antenna systems.We can think about the way that each of these limits of line broadening phenomena affects the energy transfer rate in a simple donor−acceptor systems as follows. The fast fluctuations broaden homogeneously the donor emission and acceptor absorption spectra of each member of the ensemble. Looking inside the ensemble average, static disorder affects the spectral overlap by shifting each donor emission and acceptor absorption maximum with respect to each other. This looks indistinguishable from the homogeneous line broadening in an ensemble average absorption or emission spectrum but leads to a distribution of energy transfer rates for the ensemble of donor−acceptor pairs. We can summarize this by noting that the donor emission spectrum is written $\langle f_{\mathrm{D}}^{\mathrm{hom}}(\epsilon)\rangle$, the acceptor absorption as $\langle a_{\mathrm{A}}^{\mathrm{hom}}(\epsilon)\rangle$, where the angular brackets denote ensemble average over the slow bath variables. Then we furthermore note that the Förster spectral overlap is also an ensemble average quantity, and in general $J(\epsilon) = \langle f_{\mathrm{D}}^{\mathrm{hom}}(\epsilon)\cdot a_{\mathrm{A}}^{\mathrm{hom}}(\epsilon)\rangle \neq \langle f_{\mathrm{D}}^{\mathrm{hom}}(\epsilon)\rangle\cdot\langle a_{\mathrm{A}}^{\mathrm{hom}}(\epsilon)\rangle$. A simple analytical equation for such a separation of homogeneous and inhomogeneous line broadening contributions to the Förster spectral overlap integral can be derived for the case of a simple donor−acceptor pair, as has been described by Jean and coworkers.[98] However, as we shall show in section VI, when the energy acceptor (and/or donor) is intrinsically multichromophoric, the effect of disorder is nonintuitive and such an approach fails.

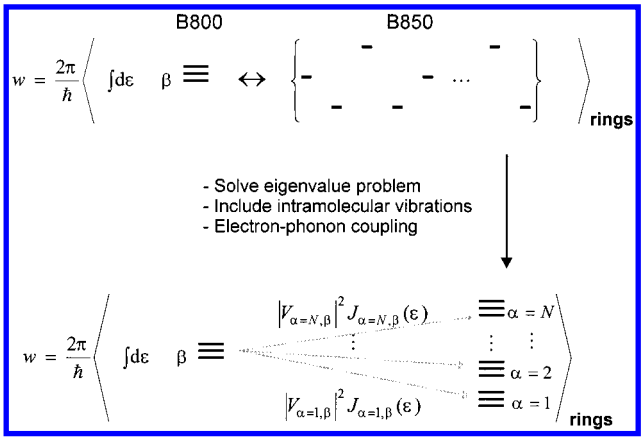

Figure 4. Schematic depiction of the model for calculating B800−B850 energy transfer described in section IV. Static disorder is introduced to the B850 BChl excitation energies in the site representation. The eigenvalue problem for each B850 ring is then solved prior to the introduction of electron−phonon coupling and intramolecular vibrational information. B800−B850 energy transfer rates are determined in the exciton representation. Ensemble averaging is undertaken over many LH2 rings.

The spectral inhomogeneity of antenna pigments in LH2 and implications for light harvesting have been considered previously.[11,99−103] These studies, however, are based on the Pauli master equation, that is, a Markovian random walk among the heterogeneous distribution of localized excitations. This is qualitatively different from the procedure we describe in the present work. To accommodate the strong coupling among the B850 chromophores, we have devised the scheme summarized in Figure 4 and described in detail below. We employ a weak coupling (Förster; Fermi Golden Rule) rate expression for the B800−B850 energy transfer. However, to account for the strongly coupled B850 chromophores and to elucidate the impications of this coupling − for example, the role of the upper exciton band of the B850 absorption − we need to be careful to implement the theory correctly, particularly because of the effects of disorder. The way that we go about this is to ensemble average over many LH2 rings using a Monte Carlo procedure. For each ring we add site disorder to the 18 B850 BChls then solve the eigenvalue problem to obtain the B850 exciton states (labeled α in Figure 4). We then calculate the electronic coupling between B800 and each exciton state and determine each energy transfer rate. It is easily shown that when the coupling between the acceptor molecules is small relative to the electron−phonon coupling (and we neglect disorder and assume a dipole−dipole coupling mechanism) the expression reduces to the Förster equation.

In the present study, we use the line shape function $g(t)$, defined in terms of the correlation function for the fluctuating

contribution to the electronic energy gap,[104,105] $M(t) = \langle \delta\epsilon_i(0)\, \delta\epsilon_i(t)\rangle / \langle \delta\epsilon_i^2\rangle$, as described elsewhere.[54,104] This provides the "homogeneous" contribution to the line-shape that is important for (i) providing the primary contribution to the spectral overlap and (ii) dynamic localization of the excitation in the B850 acceptor absorption.[29,106] Accurate account of intramolecular vibrations coupled to electronic transitions is important because of the minimal four-level model required to treat the energy transfer problem. Thus, vibronic transitions are crucial for energy conservation, especially in "downhill" energy migration. The energetic disorder represents fluctuations that are slow compared to the time scale for energy transfer and contributes an offset to the mean electronic energy gap of each BChl molecule, i.e., (in the site representation) ϵ_0 such that $\epsilon_i = \epsilon_0 + \delta_i$. The offset frequencies are assumed to have a Gaussian distribution with standard deviation σ, i.e., $P(\delta_i) = \exp(-\delta_i^2/2\sigma^2)/(\sigma\sqrt{2\pi})$. With this in mind, we introduce here the concept of an ensemble average spectral overlap and EET hopping time.

The ensemble average spectral overlap is written as

$$J(\epsilon) = \langle \sum_{\alpha} N_a a_{\mathrm{A}}^{\mathrm{hom}}(\epsilon)\, N_f f_{\mathrm{D}}^{\mathrm{hom}}(\epsilon)\rangle \qquad (7)$$

and the ensemble average rate of energy transfer from D to A is given by

$$w = \frac{2\pi}{\hbar}\langle \int_0^{\infty} \mathrm{d}\epsilon \sum_{\alpha} |V_{\mathrm{DA}}(\alpha)|^2 N_a a_{\mathrm{A}}^{\mathrm{hom}}(\epsilon)\, N_f f_{\mathrm{D}}^{\mathrm{hom}}(\epsilon)\rangle \qquad (8)$$

where $V_{\mathrm{DA}}(\alpha)$ is the electronic coupling between the donor and eigenstate α of the acceptor, and N_a and N_f are area-normalization factors relating to the donor emission and acceptor absorption density of states (DOS) line shapes, $f_{\mathrm{D}}^{\mathrm{hom}}$ and $a_{\mathrm{A}}^{\mathrm{hom}}$ (see below). Note that these line shapes together determine the density of states responsible for energy conservation via their overlap and are therefore independent of the "allowedness" of the transitions. The information dealing with the weighted contribution of each J_α is accounted for in the electronic coupling factors by virtue of the explicit separation of electronic and nuclear factors in eq 1. For instance, if a transition is dipole forbidden, then V^{Coul} will be very small since it would contain only higher multipole contributions. The same is of course true of triplet−triplet energy transfer.[69] Thus, solely a large J_α is not enough to guarrantee a significant contribution to the energy transfer rate because each J_α is associated with an electronic coupling factor $|V_\alpha|^2$. Hence, in the present work it turns out to be more revealing to consider the origin of the B800−B850 spectral overlap in terms of B800 emission and the B850 absorption band density of states weighted by the associated electronic coupling factor: $\sum_\alpha |V_\alpha|^2 J_\alpha(\epsilon)$. This has also been recognized in the work of Sumi.[107,108]

The acceptor (B850) eigenstates are given in terms of the monomer wave functions ψ_m as $\Psi_\alpha = \sum_m \varphi_m(\alpha)\psi_m$ by solving the $m \times m$ eigenvalue problem for the acceptor aggregate, with energetic disorder in the site energies ϵ_m. The coupling is thus written in terms of the eigenvector coefficients $\varphi_m(\alpha)$ and electronic couplings which are given in a site representation, $V_{\mathrm{DA}}(m)$: $V_{\mathrm{DA}}(\alpha) = \sum_m \varphi_m(\alpha) V_{\mathrm{DA}}(m)$. Recently Sumi and coworkers[107,108] have shown independently that when the excited states of the donor and/or acceptor are excitonic, and if donors and acceptors are closely separated, then it can be important to calculate donor−acceptor interactions in a monomer basis, as we have done in the present work. This is, in a sense, an extension of the monopole approximation; expressing the reduced information contained in the transition moment of a delocalized eigenstate in terms of the transition moments on each molecule that comprises the aggregate (i.e., each bacteriochlorophyll in the B850 ring).

The area-normalized B800 donor fluorescence line shape for the donor D is defined by

$$f_{\mathrm{D}}(\epsilon) = \langle N_f |\mu_{\mathrm{D}}|^2 \sum_k P(k) \mathrm{Re} \int_0^{\infty} \mathrm{d}t \langle k|k(t)\rangle \exp[i(\epsilon - \bar{\epsilon}_{\mathrm{D}}^k + \lambda)t/\hbar] \exp[-g^*(t)]\rangle \epsilon^3 \qquad (9)$$

where it is assumed that vibrational relaxation and thermalization have occurred prior to emission (and therefore prior to energy transfer). λ is the reorganization energy associated with the Stokes shift. The situation where a time-dependent Stokes shift of the donor emission occurs on a time scale comparable to that for energy transfer has been addressed previously by Mukamel and Rupasov.[109] We also assume here that excitation is localized on a single BChl chromophore in the B800 (donor) ring, which is reasonable given the small B800−B800 coupling of 30 cm^{-1}. However, by making this assumption, we neglect any effects of spectral diffusion within the inhomogeneously broadened B800 band.[7,11,25,110−113] N_f is a normalization constant such that $1/N_f = \int_0^{\infty} \mathrm{d}\epsilon f_{\mathrm{D}}^{\mathrm{hom}}(\epsilon)$, where the superscript "hom" specifies the line shape in the absence of disorder; in other words, eq 9 could be written $f_{\mathrm{D}}(\epsilon) = \langle N_f |\mu_{\mathrm{D}}|^2 f_{\mathrm{D}}^{\mathrm{hom}}(\epsilon)\rangle \epsilon^3$. μ_{D} is the donor transition moment, k labels the vibrational modes, and $\langle k|k(t)\rangle$ represents the time-dependent overlap of the initial vibration k with its evolution in the excited electronic state, as described in detail elsewhere,[114−118] which is a time-domain representation of the Franck−Condon factors. $\bar{\epsilon}_{\mathrm{D}}^k$ is the electronic energy gap of the donor molecule, adjusted for thermal population of mode k in the excited electronic state. It contributes with Boltzmann weighting $P(k)$. The angular brackets denote an ensemble average over the static disorder in the site energies. In practice, this is achieved by a Monte Carlo procedure as described by Fidder et al.[119]

The B850 acceptor, A, absorption spectrum is defined by the ensemble average of the sum over eigenstates α,

$$a_{\mathrm{A}}(\epsilon) = \langle \sum_{\alpha} N_a |\mu_\alpha|^2 \sum_l P(l)\, \mathrm{Re} \int_0^{\infty} \mathrm{d}t \langle l|l(t)\rangle \exp[i(\epsilon - \epsilon_\alpha^l - \lambda)t/\hbar] \exp[-g(t)]\rangle \epsilon/n \qquad (10)$$

where l denotes the vibrational modes of the ground state, n is the number of acceptor molecules in the aggregate (18 in the present case), and the area normalization is given by $1/N_a = \int_0^{\infty} \mathrm{d}\epsilon a_{\mathrm{A},\alpha}^{\mathrm{hom}}(\epsilon)$ for eigenstate α. Once again, we can write $a_{\mathrm{A}}(\epsilon) = \langle \sum_\alpha N_a |\mu_\alpha|^2 a_{\mathrm{A}}^{\mathrm{hom}}(\epsilon)\rangle \epsilon/n$. Notice that the index α, specifying the eigenstate, is implicit in both N_a and $a_{\mathrm{A}}^{\mathrm{hom}}(\epsilon)$. It is assumed that bath fluctuations at each site are uncorrelated and have the same spectral density, as suggested by other workers.[29,55,120−122]

V. Summary of Input Parameters

In the present work, we report calculations modeling energy transfer within the peripheral light harvesting complex LH2, focusing on the purple nonsulfur bacterium *Rhodobacter sphaeroides*. We have attempted to use the most realistic parameters possible; therefore, all were obtained by modeling experiment or from sophisticated quantum chemical calculations (e.g., we never employ the dipole approximation or phemonological line shape models). None of the paramers are adjusted. We label the BChl-*a* bound to the α transmembrane α-helix as α and that bound to the β α-helix as β. We associate these BChls with site energies $E_\alpha = 12\,600$ cm^{-1} (794 nm) and E_β

$= 12\,070$ cm^{-1} (828 nm) by modeling the 77 K absorption and circular dichroism (CD) spectra. The electronic couplings have been determined using ab initio quantum chemical methods based on the X-ray crystal structure data of *Rhodopseudomonas acidophila* strain 10050,[1,2] and are reported in refs 36 and 37. The electronic couplings within the B850 ring are $V_{\alpha-\beta-\text{intrapolypeptide}} = 320$ cm^{-1}, $V_{\alpha-\beta-\text{interpolypeptide}} = 255$ cm^{-1}, $V_{\alpha-\alpha} = -48$ cm^{-1}, and $V_{\beta-\beta} = -37$ cm^{-1}. The principal assumption that we have made for the *Rb. sphaeroides* calculations is that the electronic couplings and transition moment orientations in this bacterium are the same as those for *Rhodopseudomonas acidophila* strain 10050. We have ascertained that this assumption is reasonable by calculating the absorption and CD spectra for the B850 band (Figure 2) and finding a satisfactory correspondence to these data for the B800-deficient mutants reported by Koolhaas et al.[19] and the calculations reported by those workers.[20]

B800−B850 couplings are those reported in ref 37. The B800 donor is assumed to be monomeric, absorbing at 800 nm, with a Stokes shift of 130 cm^{-1}. Transition moment directions and molecular centers were taken from the *Rps. acidophila* strain 10050 crystal structure data.[1,2] We assume that the LH2 rings are circular, as suggested by the X-ray structure data, although a recent single molecule study indicates the possibility that some rings could be elliptical.[123] The line shape functions were determined from analysis of three pulse stimulated echo peak shift (3PEPS) data[88,89] and are defined by the electronic energy gap correlation function $M(t) = \lambda_1 \exp[-(t/\tau_1)^2] + \lambda_2 \exp(-t/\tau_2)$ with $\lambda_1 = 32$ cm^{-1}, $\tau_1 = 40$ fs, $\lambda_2 = 21$ cm^{-1}, and $\tau_2 = 15$ ps.[124] Here λ_i and τ_i are the coupling strengths and time scales characteristic of the bath. Intramolecular vibrational frequencies and dimensionless displacements were taken from the literature and implemented into our line-shape functions using the time-dependent formalism of Lee and Heller.[114−118] We used, for both B800 and B850 BChls (frequency, cm^{-1}; dimensionless displacement): (110; 0.0), (166; 0.14), (194; 0.2), (342; 0.14), (564; 0.2), (650; 0.14), (750; 0.3), and (920; 0.3) as used by Pullerits et al.[18] which were derived from previous work.[97,125] Each calculation employed 1000 to 2000 iterations over the site energy disorder (in E_α, E_β, and E_{B800}), which was taken to have a Gaussian distribution with a standard deviation of $\sigma = 160$ cm^{-1} for E_α and E_β, and $\sigma = 93$ cm^{-1} for E_{B800} determined from analysis of 3PEPS data.[126]

VI. Ensemble Averaging and B800−B850 Energy Transfer Dynamics

It is evident from the single molecule fluorescence excitation spectra reported by van Oijen et al.[123] that site inhomogeneity makes the B850 absorption band of each LH2 ring look quite distinct. To account for effects such as this inhomogeneous distribution of acceptor states, we have employed the scheme shown in Figure 4 and described above. This procedure is illustrated further in Figure 5, which displays the result of our calculations for just one LH2 ring. For this ring, Förster theory would dictate that the overlap integral be determined by the B800 emission and B850 absorption. We have described above the reasons that this is not so when the donor and/or acceptor is multichromophoric, and in fact we therefore derive a spectral overlap, summed over all acceptor eigenstates, $\sum_\alpha J_\alpha(\epsilon)$ from the B850 density of states. We then find the rate of energy transfer in this individual LH2 complex to be determined by the coupling-weighted spectral overlap: $\sum_\alpha |V_\alpha|^2 J_\alpha(\epsilon)$. We repeat this procedure 1000−2000 times to ensemble average over many LH2 rings.

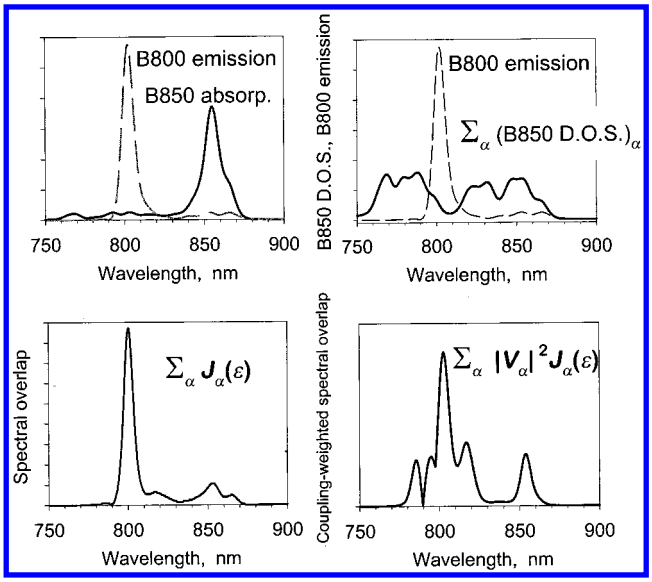

Figure 5. A detailed depiction of quantities calculated for a single LH2 ring to illustrate the model shown in Figure 4 and described in the text.

In Figure 6, the results of calculations of B800 emission spectra, B850 absorption spectra, and spectral overlaps for B800 donor−B850 acceptor (at 100 K) are shown. These have been calculated using eqs 9, 10, and 7, respectively. We have chosen to report the 100 K calculations because the results illustrate most clearly the effect of disorder (because the "homogeneous" line width is narrower than at 300 K). However, the 300 K calculations reveal the same features. We compare the case where coupling between the B850 BChls is ignored (parts a and b of Figure 6) and that with coupling in the B850 ring (parts c and d of Figure 6). Note that the B850 BChl site energies are artificially red-shifted to obtain the spectra with no coupling. This is simply to try to compare the "with" and "without" coupling calculations on equal footing. Absorption spectra of B850 calculated for 20 K and with no disorder are also shown for both no electronic coupling between the B850 BChls (Figure 6a) and coupled B850 BChls (Figure 6c), which show the positions of the vibronic bands (cf. 6a) and the upper exciton band at approximately 777 nm (6c) which is evident when coupling is considered. Notice also that the B850 main absorption band is narrower when the BChls are coupled (Figure 6c) compared to the uncoupled case (Figure 6a). This is characteristic of exchange narrowing.[127] That is, coupling delocalizes the excitation over many molecules in an aggregate, which in turn causes the excitation to average over the local inhomogeneities of these sites. This leads to a reduction of the inhomogeneous width of the absorption line.

The spectral overlaps $J(\epsilon)$ for each case are shown in parts b and d of Figure 6. The dashed−dotted line in Figure 6b illustrates a calculation of $J(\epsilon)$ for the situation where the B850 BChls are uncoupled and disorder is ignored; this is considered to be the "normal" Förster overlap calculation (cf. eq 1). It is compared to the corresponding ensemble average calculation (i.e., by adding account of the disorder), clearly showing the differences. The overlap integrals, $J = \int_0^\infty d\epsilon\ J(\epsilon)$, were calculated to be $J = 1.19 \times 10^{-4}$ cm (no disorder, no couplings in the B850 ring) and $\langle J \rangle = 3.03 \times 10^{-4}$ cm (ensemble average over site energy disorder, no couplings in the B850 ring). The marked difference in $J(\epsilon)$ when the couplings between B850 BChls are considered is seen in Figure 6d. The ensemble average spectral overlap here is determined to be $\langle J \rangle = 2.83 \times 10^{-4}$ cm (ensemble average over site energy disorder, couplings in the

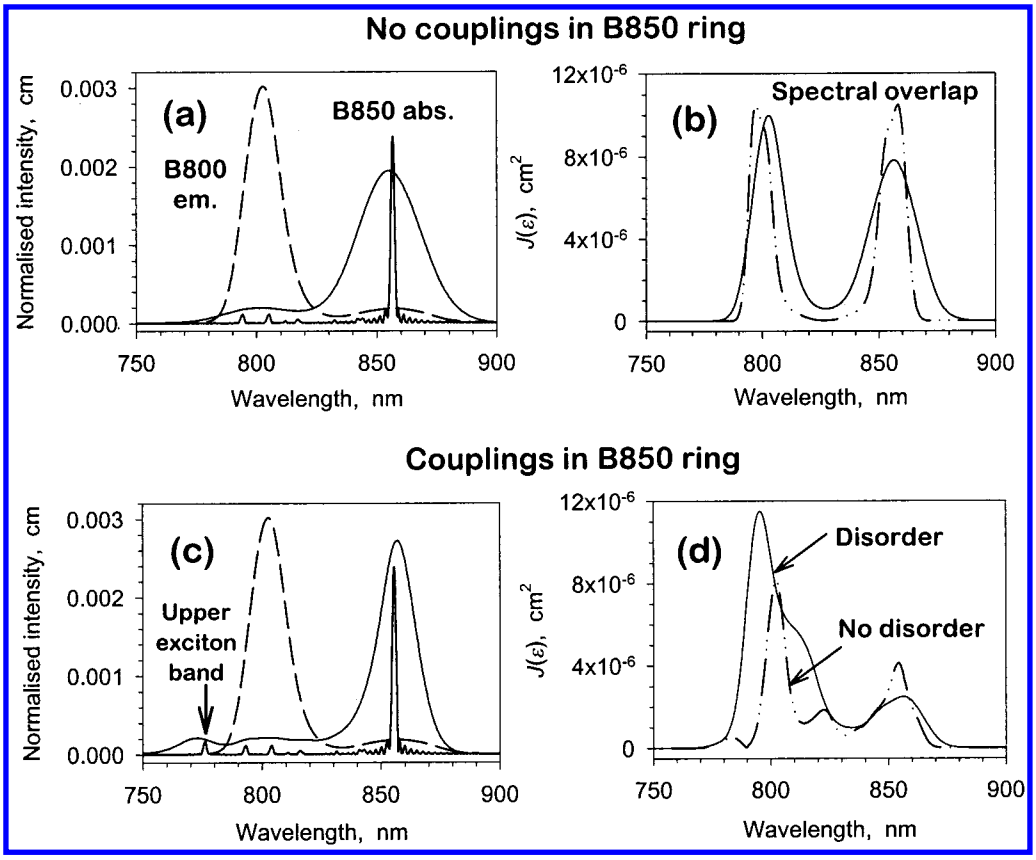

Figure 6. Results of the calculations for *Rb. sphaeroides* LH2 at 100 K. The two upper panels are the results of calculations based on a Hamiltonian which contains zero couplings between the B850 BChls, and with the BChl site energies red-shifted so that the absorption band is centered at 857 nm. (a) B800, donor, emission spectrum (dashed line) and B850, acceptor, absorption spectrum (broad solid line). The narrow solid line is the B850 absorption calculated at 20 K *without disorder*. (b) The solid line is the corresponding ensemble average spectral overlap. The dashed−dotted line is the spectral overlap with no disorder (i.e., this is the "Förster" result). The two lower panels are the results of calculations based on the Hamiltonian described in the text which contains couplings between the B850 BChls. (c) Analogous to (a). The position of the upper exciton band is indicated. (d) Analogous to (b).

B850 ring), which again is approximately twice that calculated in the absence of disorder, $J = 1.49 \times 10^{-4}$ cm (no disorder, couplings in the B850 ring). Hence, we see here that the disorder of the site energies (of both B850 and B800 BChls) has a crucial influence on the B800 to B850 energy transfer rate via the spectral overlap.

The primary conclusion we draw from these investigations is that the *spectral overlap is an ensemble average quantity* and has a profound effect on the energy transfer time when disorder contributes to the absorption/emission line shapes. The effect of varying the magnitude of the disorder is shown in Figure 7. Furthermore, we emphasize that the $J_\alpha(\epsilon)$ for eigenstate α of B850 is weighted by the electronic coupling between B800 and α. This weighted spectral overlap is plotted in Figure 7c. With all other quantities being equal, increasing the disorder increases the energy transfer rate through its influence on the spectral overlap integral. As suggested in Figure 5, this is promoted by increasing the B850 oscillator strength in the upper exciton region (ca. 780 nm) of the spectrum (particularly around 800 nm), thus increasing the $J(\epsilon)$ under the B800 emission. The way that this works can be understood by looking at contributions to the ensemble average, for example the "single molecule" spectra shown in Figure 8 (all calculated for 100 K). These are three random contributions to the ensemble average B850 absorption spectrum and the corresponding B800−B850 coupling-weighted spectral overlap. It is evident that disorder in the B850 site energies tends to shift the B850 density of states to give better overlap with the B800 band (and the same holds for disorder in the B800 transition energy), which in turn enhances the $J(\epsilon)$ and $\sum_\alpha |V_\alpha|^2 J_\alpha(\epsilon)$ at around 800 nm compared to that in the 850 nm region. As an aside, it has not escaped our attention that the aborption spectra of the B850 rings in Figure 8a looks very similar to some of the "unusual" single molecule LH2 fluorescence excitation spectra reported by van Oijen et al.[123] We return to this point is section IX.

The disorder-induced broadening of the density of acceptor states in the B850 band is depicted in Figure 9, where we compare the ensemble average B850 density of states with that calculated in the absence of disorder. It is evident that the "hole" in the density of states at about 800 nm is filled in by the disorder, thus increasing the spectral overlap with B800. We also show in Figure 9 the B850 density of states calculated for the case of no couplings between the BChls in the B850 ring (as in parts a and b of Figure 6). Comparison of parts a and c of Figure 9 shows immediately why the spectral overlaps calculated "with" and "without" couplings, parts b and c of Figure 6, respectively, have such different shapes. Hence, a key role played by the electronic couplings in the B850 ring is to increase spectral coverage of the B850 energy acceptor density of states. Comparing parts a and c of Figure 9 suggests that the couplings act to spread the significant density of states from 830−870 nm to 760−870 nm. It would be very difficult to achieve this with disorder only.

The results of our calculations of the ensemble average spectral overlap integrals, as well as energy transfer times for these different model cases are summarized in Table 1 (for both

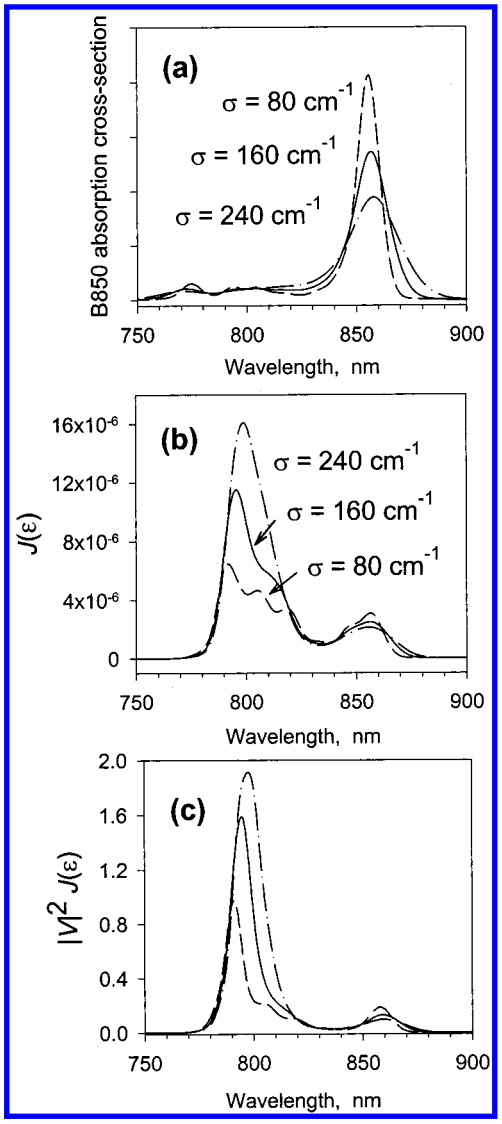

Figure 7. (a) The B850 absorption spectrum, (b) B800−B850 spectral overlap, and (c) the coupling-weighted spectral overlap calculated at 100 K for different amounts of disorder in the B850 BChl site energies. That for the B800 chromophore was fixed at $\sigma = 93$ cm^{-1}.

$T = 100$ and 300 K). We can now compare the changes in rate of B800 to B850 energy transfer with changes in spectral overlap integral, with and without coupling within the B850 BChls. The Förster equation, eq 1, naturally suggests that if the electronic coupling between donor and acceptor, V, is constant, then the rate of energy transfer must vary proportionally to the spectral overlap integral, J (i.e., $w_1/w_2 = J_1/J_2$ if $V_1 = V_2$). This is confirmed by comparing (for the uncoupled B850 acceptor ring) the ratio of rates with and without disorder (columns A and B in Table 1), w(B)/w(A) with the corresponding ratio of spectral overlap integrals, J(B)/J(A); w(B)/w(A) = 2.53 versus J(B)/J(A) = 2.55 for our calculations at 100 K.

We can highlight the influence of taking proper account of electronic couplings within the B850 acceptor ring for the case where there is no disorder, w(C)/w(A) = 0.682 versus J(C)/J(A) = 1.25 at 100 K. Here, a significant deviation from the expectation of the Förster equation is evident. When disorder is included in the calculation, we obtain w(E)/w(B) = 0.882 versus J(E)/J(B) = 0.934 for 100 K. Now we notice that the ratios are more similar than they are in the absence of disorder. This is simply because the effect of disorder is to enhance localization of the excitation, thus making the B850 acceptor

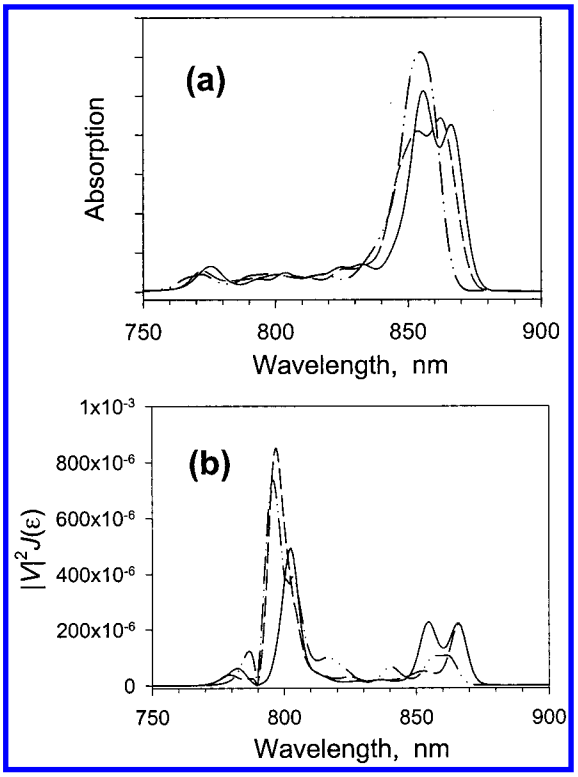

Figure 8. Three "single molecule" calculations (*Rb. sphaeroides*, 100 K) taken at random from the ensemble average. (a) The B850 "single molecule" absorption spectra and (b) the B800−B850 coupling-weighted spectral overlaps. Note the marked effect that disorder has on both these quantities.

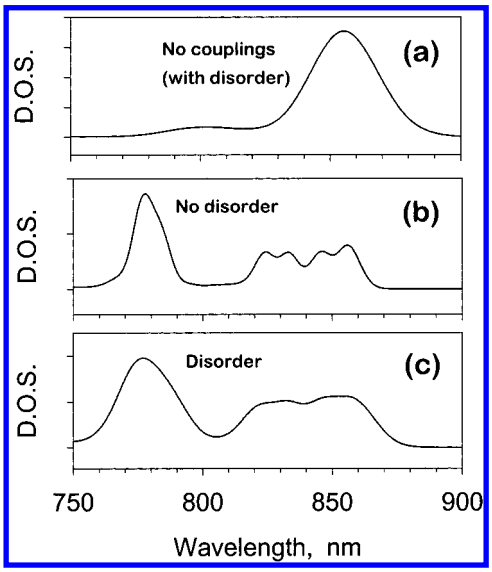

Figure 9. Calculated B850 band density of states (*Rb. sphaeroides*, 100 K) for (a) ensemble average with disorder, but no couplings between the B850 BChls; (b) no disorder, but with couplings in the B850 ring; (c) ensemble average with disorder, and with couplings in the B850 ring. The disorder evidently "fills in" the gap in the acceptor density of states in the 800 nm region. The couplings lead to a broad spectrum of acceptor states.

more "monomer-like".[11,22,26,31,38,128−132] In Figure 10, we plot both the rate of EET and the spectral overlap integral versus temperature, thus showing clearly the different temperature dependences of w and J which arise owing to the excitonic structure of the acceptor transitions.

Considering these results, we conclude that the B850 ring is a fairly complex energy acceptor. To model the B800−B850

TABLE 1: Results of the B800−B850 Energy Transfer Calculations for LH2[a]

calculation	A	B	C	D	E[b]	F
B850 couplings?	no	no	yes	yes	yes	yes
σ, cm^{-1} [c]	0	160	0	80	160	240
			100 K			
J, μm[d]	1.19	3.03	1.49	2.13	2.83	3.59
w, ps^{-1} [e]	0.220	0.557	0.150	0.316	0.491	0.656
τ, ps[f]	4.55	1.80	6.68	3.17	2.04	1.53
			300 K			
J, μm	3.31	2.90	2.61		3.69	
w, ps^{-1}	0.609	0.534	0.426		0.673	
τ, ps	1.64	1.87	2.35		1.48	

[a] Calculations for *Rb. sphaeroides*. [b] Column E relates to experiment. [c] The standard deviation of the site energy disorder refers to B850. When this is nonzero, the B800 disorder is always 93 cm^{-1} (unless $\sigma_{B850} = 0$, then $\sigma_{B800} = 0$). [d] Spectral overlap integrals $J = \int_0^\infty d\epsilon\, J(\epsilon)$, cf. eq 7. The units are more familiar as $10^{-4} \times$ cm $\equiv 1$ μm. [e] Energy transfer rate, eq 8. [f] Energy transfer time, $\tau = 1/w$. These energy transfer times have not been scaled according to the dielectric screening of the protein, which would increase them (i.e., slow the rate) by approximately 25%.

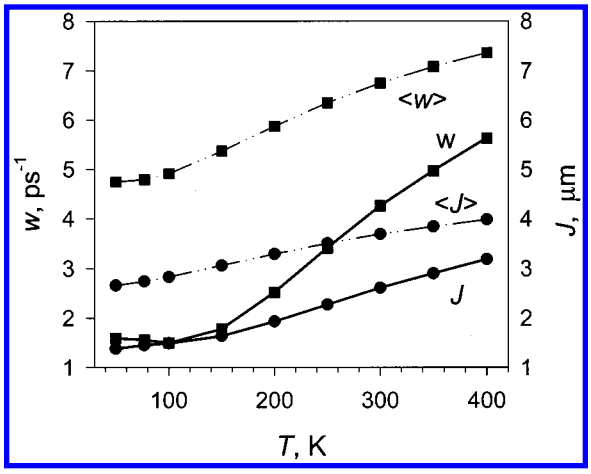

Figure 10. Calculated temperature dependences of both the EET rate, w, and the spectral overlap, J, for B800−B850 energy transfer (a) with no disorder, solid lines, and (b) with disorder, dash−dot lines. Note that the simple relationship between w and J that is suggested by the Förster equation does not hold.

energy transfer, we needed to include every B850 BChl chromophore in the simulation; however, previous work has suggested that the excitation is localized on the time scale of the energy transfer transition to approximately three chromophores.[11,22,26,31,38,128−132] This is not an oxymoronic statement but shows that the electronic wave function is sensitive to the structure of the aggregate, but the spectroscopic properties, which relate to the density matrix, are localized relative to the bare electronic states by electron−phonon coupling and disorder. The reasoning behind this is suggested by the work of Sauer et al.[14] where it is shown that the full B850 ring must form the basis for calculation of the absorption or CD spectra. This is simply because we need the full structural basis set in order to calculate the electronic wave functions. We attribute the temperature dependence of the EET rate, particularly in the absence of disorder, principally to changes in the delocalization length of the B850 acceptor band.

In Figure 11, we compare the temperature dependence of $J(\epsilon)$ for the case of (a) no disorder with that (b) where we have included disorder (i.e., the ensemble average calculation). It is seen clearly that it is the disorder that is responsible for the weak temperature dependence of the B800 to B850 energy

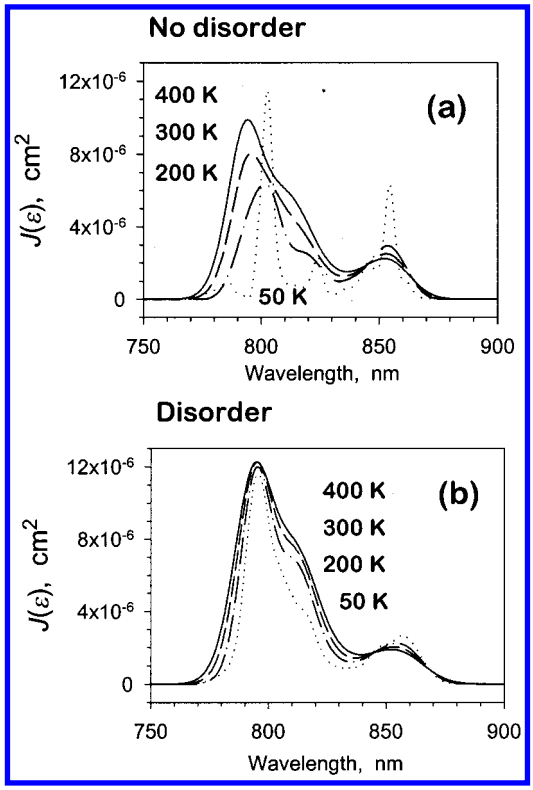

Figure 11. Temperature dependences of the B800−B850 spectral overlaps for (a) no disorder and (b) with disorder. It is clearly seen that the effect of disorder is to temper the temperature dependence.

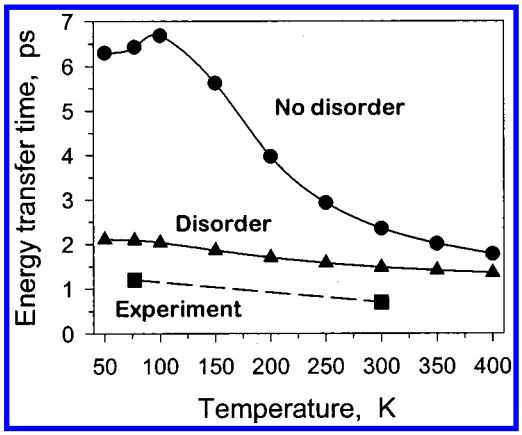

Figure 12. Comparison of the temperature dependence of the B800−B850 energy transfer time for calculations (i) with no disorder; (ii) with disorder, but with no account of the carotenoids; and (iii) the experimental results for *Rb. sphaeroides*.

transfer time, via the ensemble average spectral overlap. This is illustrated in Figure 12, where the corresponding energy transfer times are plotted as a function of temperature. Evidently it is the influence of disorder that dictates the weak temperature dependence of the energy transfer time.

The calculated B800−B850 energy transfer times, though significantly closer than previous estimates to those measured experimentally,[11,18,40−47] are still too slow by a factor of about two both at 300 K and 77 K. (Note also that dielectric screening, eq 6, has not yet been included in these results.) We address one reason for this in the following section, then describe the limitations of our model in section VIII. In section IX, we report calculations on *Rps. acidophila* and a series of reconstituted complexes, which suggest that we could have obtained close agreement with the actual energy transfer rates, in addition to

the temperature dependence, for *Rb. sphaeroides* by making small adjustments to the B850 site energies.

VII. Role of the Carotenoids

It has been postulated previously that the discrepancy between measured and calculated B800 to B850 energy transfer times could be in part resolved by accounting for superexchange-mediated coupling via the carotenoids.[18,60] In other words, the through-space electronic couplings from B800 to B850 may be augmented by a coupling through the π/π^* system of the bridging carotenoids. Such superexchange-mediated triplet−triplet energy transfer has been observed previously, for example in isotopically doped mixed crystals[84] and in bichromophores.[133,134] More recently, there have been reports of singlet−singlet energy transfer rates being increased by through-bond contributions to the coupling.[82,135,136] In particular, the recent work of Kilså et al.[136] highlights the expected[137−139] increase in EET rate as the electronic energy gap between the donor and the bridge decreases. Superexchange-mediated through-bridge triplet−triplet EET is promoted primarily by charge transfer resonance interactions[67] (that depend explicitly on orbital overlap between donor-bridge and bridge-acceptor). Such a mechanism contributes also to superexchange-mediated through-bridge singlet−singlet EET, especially for the all-trans polynorbornane bridges.[82,135] In addition, a contribution from a Coulombic coupling is expected,[82,83,137] particularly when the bridge has a low-lying and strongly allowed transition that couples to the donor and acceptor transitions. We examine these two possibilities here for the B800-carotenoid-B850 coupling.

We describe the interactions between the electronic transitions of the BChl and the carotenoid in the manner suggested by Robinson,[140] see Appendix, where it is shown that the transition moment of the BChl may be perturbed by the presence of the carotenoid. Calculations of the excited states of strongly interacting dimers, moreover, have shown that mixing of the CT configurations into the locally excited configurations also perturbs the dimer transition moment when interchromophore orbital overlap is large.[141] (Note that in these strongly coupled dimer systems we cannot set $N \approx 1$.) This has been observed experimentally in the enhancement of superradiant radiative rates of model bisnaphthalene molecules which were correlated with enhanced polarizabilities determined using time-resolved microwave conductivity.[142] Considering all these effects, we obtain eq 11.

$$\vec{\mu}_{m0;00} \approx \vec{\mu}^{\mathrm{M}}_{m0} + \lambda\vec{\mu}_{+-;00} + \mu\vec{\mu}^{-+;00} + \sum_p \eta_p \vec{\mu}^{\mathrm{P}}_{p0} \quad (11)$$

where the mixing coefficients λ and μ have been given previously[76] and the η_p are given by Robinson (terms X and XI of eq 8 of that paper[140]). Approximate expressions are provided in the appendix.

We have undertaken an analysis of the B800−B850 energy transfer time, absorption spectrum and CD spectrum using an extended Hamiltonian based on eq A2 (with $\lambda = \mu = 0$ and η given by the leading term in eq A6) that included the nine carotenoids in LH2 and their Coulombic couplings to the B850 and B800 BChls (taken from ref 37). However, the results were found to be quite similar to those described in section VI; that is, the calculated B800−B850 energy transfer time was not significantly increased.

More detailed, ab initio quantum chemical, calculations of carotenoid-mediated B800−B850 electronic coupling in LH2 have been reported recently.[39] These calculations reveal that the transition densities of both the B800 and B850 BChls are significantly perturbed by interaction with the carotenoid. The transition density is both shifted and tilted with respect to that of an unperturbed BChl *a*, for example as shown in Figure 13. The origin of this interaction is unknown, but presumably the Coulombic coupling between BChl and carotenoid is important. If this were so, then the analysis described above, which is based on eq 11 with $\lambda = \mu = 0$ and η given by the leading term in eq A6, would reveal a significant effect on the rate of B800−B850 EET owing to superexchange-mediated contributions to the electronic coupling. In fact, the calculations reported by Krueger et al.[39] suggest that the B800−B850 couplings are increased by over 50% in the presence of the bridging carotenoid, owing to changes in the separations and orientation factors of the B800−B850 transitions. It is likely that a more detailed description of the carotenoid polarizability and its contribution to eq 11 is required. However, just as the CI-singles transition densities need to be scaled owing to the neglect of electron correlation at this level of theory, the BChl-carotenoid mixing should also be scaled. Using eq A6 and the dipole approximation for $V_{0p;m0}$, we can determine the approximate scaling relation based on second-order perturbation theory: $\eta_p^{\mathrm{CIS}}/\eta_p^{\mathrm{exp}} \approx (9.7 \times 24.1\ \mathrm{Debye}/3710\ \mathrm{cm}^{-1})/(6.13 \times 13.0\ \mathrm{Debye}/5680\ \mathrm{cm}^{-1})$. This suggests that the CI-singles supermolecule calculation overestimates the perturbation of the BChl transition moments and, in turn, the B800−B850 couplings owing to overestimation of the monomer transition moments (which has already been accounted for by the scaling procedure used by Krueger et al.[39]) and underestimation of the BChl Q_y to carotenoid S_2 energy gap.

We conclude that the B800−B850 couplings are increased by approximately 20−30% via mixing of the BChl and carotenoid transition moments. The results of these calculations may offer an explanation as to why the CD spectrum in Figure 2 differs from experiment in the region of the upper exciton transition. Koolhaas et al.[19] suggested that this could be resolved by tilting the transition moment of one of the B850 BChls. The transition density calculations offer a possible origin of this tilt as arising from mixing of the BChl electronic transitions with those of the carotenoids.

This result suggests another of the several roles played by the carotenoids in the LH2 complex. Without being directly involved in the B800−B850 energy transfer process, the carotenoids appear to be capable of enhancing the energy transfer rate through their involvement as bridging polarizable media. In light of these quantum chemical results, a further calculation of the B800−B850 energy transfer time for a temperature of 300 K was undertaken using B800−B850 couplings 30% larger in order to simulate the effect of the carotenoid. The results can be compared directly to the 300 K results given in column E of Table 1; all parameters in these calculations are identical except for the magnitudes of the B800−B850 electronic couplings. Thus, the spectral overlaps are the same. The calculated energy transfer rate is significantly faster, corresponding to the larger electronic couplings between donor and acceptor.

In summary, quantum chemical calculations designed to investigate possible superexchange-mediated coupling between B800 and B850 revealed that the transition densities of both the B800 and B850 BChls are perturbed by interaction with the carotenoid. They are tilted and shifted, which could be the physical basis for the postulate of Koolhaas et al.[19] that the discrepancy between calculated and measured CD spectra can be resolved by tilting the BChl transition dipole moments. A

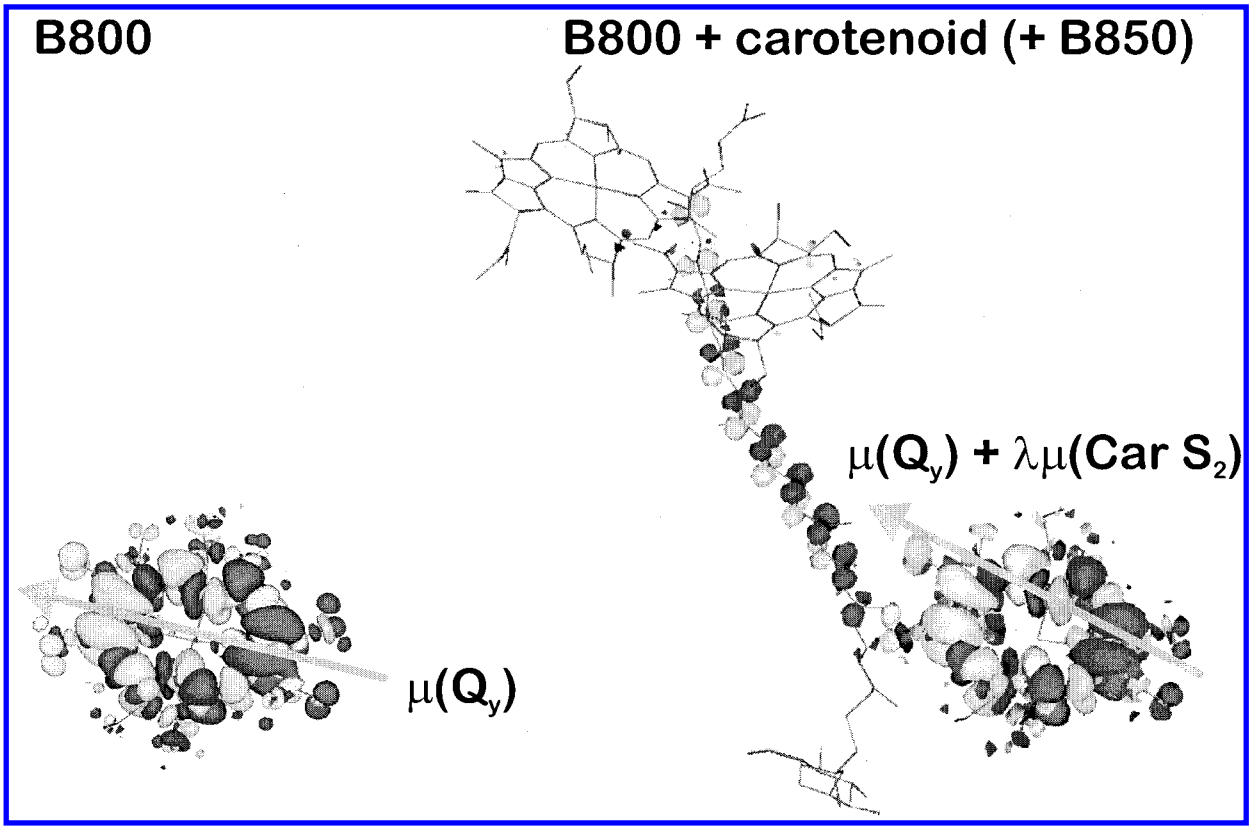

Figure 13. CIS/3-21G* transition densities for the Q_y transition of (a) an isolated B800 BChl and (b) a B800 BChl in the presence of the closest carotenoid. The corresponding Q_y dipole transition moments are shown schematically to highlight the shift of the B800 transition density owing to mixing with the carotenoid transitions.

consquence of this BChl-carotenoid interaction is that the carotenoids appear to be capable of enhancing the energy transfer rate (by ca. 50−70%) through their involvement as bridging polarizable media.

VIII. Limitations of the Model

We believe that the ensemble average energy transfer model described in this work contains the principal ingredients required to address quantitatively the B800−B850 energy transfer dynamics and mechanism. However, we list briefly here several limitations and omissions that may be addressed in future work. (i) We do not know precisely how well we have modeled the B800 emission line shape and emission maximum. (ii) Recent analysis of photon echo data in our laboratory[126] suggests that B800−B800 energy transfer occurs on a time scale as fast as 400 fs, implying that spectral diffusion among the B800 sites can occur on a time scale competitive with B800−B850 energy transfer. This is not considered in our model. (iii) It seems that the B800−B850 spectral overlap is sensitive to the relative positions of the upper exciton component of the B850 absorption band and the B800 emission band. However, it can be seen in Figure 6c that the upper exciton region overlaps very little with the B800 emission, which could be very species-dependent (e.g., comparison of *Rps. acidophila* B800−B850 with B800−B820). We have investigated this, and the results are reported in section IX. (iv) Although we have used experimentally determined line shape functions, we have employed a quite simple model for relating site spectral densities to the eigenstates. More detailed models introduce a great deal of complexity into the calculations.[120] We have also assumed that the spectral density is temperature independent. (v) We have not considered the possibility of disorder in the transition moment directions and positions. This would influence the distribution of oscillator strength in the B850 eigenstates, and hence the spectral overlap.

IX. *Rps. Acidophila* and Reconstituted Complexes

In this section, we simulate the B800−B850 energy transfer for the LH2 of *Rps. acidophila* strain 10050 as well as for a series of complexes which have been reconstituted with modified BChls replacing those removed from the B800 sites.[143−145] In these complexes, the absorption band associated with the B800 ring is shifted to different spectral regions according to the exchanged BChls. Recent work has reported the dependence of the B800−B850 energy transfer time on the position of the "B800" absorption band maximum.[146] To gain deeper insight into the calculations reported in the present work, and hence the mechanism of the B800−B850 energy transfer, we have simulated the energy transfer dynamics in the wild type *Rps. acidophila* B800−B850 complex, as well as in four reconstituted complexes in which the B800 band lies at 765, 753, 694, and 670 nm (which we refer to as B765, B753, etc.). Presumably, a good test of our energy transfer model is to be able to make predictions for different species, strains, mutants, etc.

To simulate the *Rps. acidophila* B850 band we use the same parameters as described above for *Rb. sphaeroides*, except for the BChl site energies. We set these to $E_\alpha = 12\,460$ cm^{-1} (803 nm) and $E_\beta = 12\,070$ cm^{-1} (828 nm) in order to reproduce the absorption and CD spectra. Typical single complex absorption spectra are shown in Figure 14 and are seen to compare well with the fluorescence excitation spectra reported by van Oijen et al.[123] We furthermore note that we could reproduce these single-molecule spectra without having to distort the structure of the LH2 ring (such as introducing ellipticity[123]), nor are we

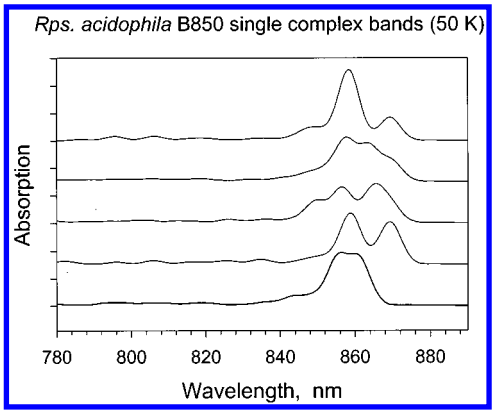

Figure 14. Five "single molecule" calculations of absorption spectra (*Rps. acidophila*, 50 K) taken at random from the ensemble average.

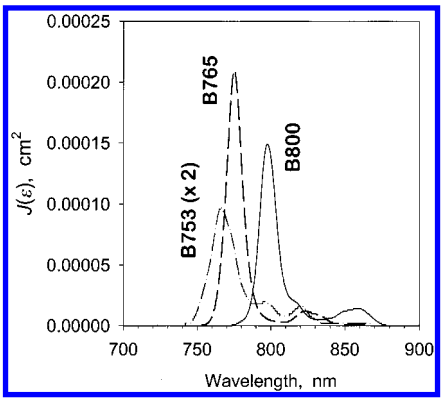

Figure 15. Spectral overlaps calculated for the wild type *Rps. acidophila* and two of the reconstituted complexes (77 K).

TABLE 2: Results of the B800−B850 Energy Transfer Calculations for LH2 and Reconstituted Complexes[a]

	no disorder		disorder		
LH2	J, μm	τ, ps[c]	J, μm	τ, ps[c]	exptl[b] τ, ps
			77 K		
B800	2.33	2.23	4.36	0.96	
B765	3.60	1.27	5.40	0.76	
B753	1.30	3.42	2.22	1.90	
B694	0.20	17.5	0.22	17.3	
B670	0.06	63.9	0.08	49.6	
			300 K		
B800	5.16	0.76	4.92	0.91	0.9
B765	4.01	1.06	5.39	0.75	1.4
B753	1.89	2.17	3.04	1.34	1.8
B694	0.22	16.9	0.27	13.8	4.4
B670	0.06	62.3	0.009	43.7	8.3

[a] Calculations of *Rps. acidophila* strain 10050 and reconstituted complexes (see text). [b] From ref 130. [c] These energy transfer times have not been scaled according to the dielectric screening of the protein, which would increase them by approximately 25%.

led to suggest that the excitation on a single LH2 ring is completely delocalized.[123]

The ensemble average spectral overlaps calculated for three of the *Rps. acidophila* complexes are shown in Figure 15 the other two (B694 and B670) are not shown because they are so small. In Table 2, we summarize the results of these calculations for both 77 and 300 K. Note that here it is assumed that each of the substituted chlorophylls has the same transition moment magnitude and orientation, and therefore coupling to the B850 BChls, as the wild-type B800s. We see from the results collected in Table 2 that (i) the calculated energy transfer times for B800−B850 and B753−B850 correspond closely to the experimental values reported by Herek et al.;[146] (ii) the calculated B694−B850 and B670−B850 energy transfer times are much slower than experiment suggests; (iii) while the "B800"-type donor has appreciable overlap with the B850 density of states, which spans 720−870 nm, the "B800"-B850 energy transfer time is rapid and is sensitive (i.e., can be tuned by a factor of 2 in magnitude) to the exact location of the donor emission spectrum (see also the spectral overlaps in Figure 15).

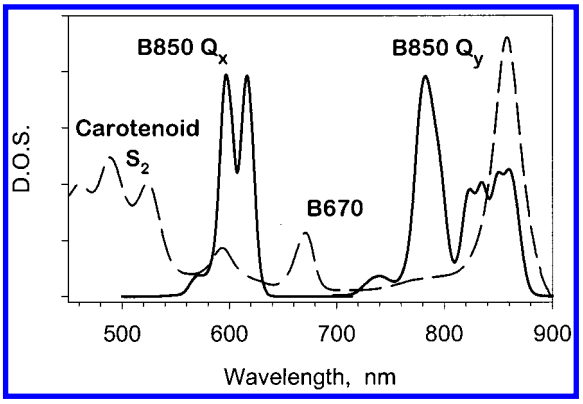

Figure 16. Calculated B850 Q_y and Q_x density of states (DOS) for *Rps. acidophila* which highlights the broad spectral window achieved by the arrangement of the B850 pigments in the LH2 complex. To put this in perspective, the absorption spectrum of the reconstituted *Rps. acidophila* B670−B850 LH2 complex (recorded at 77 K) is shown (dashed line). This spectrum shows the carotenoid (rhodopin glucoside) $S_2 \leftarrow S_0$ absorption in the spectral window to the blue side of the B850 Q_x and the 650−710 nm region, where there are no electric dipole allowed absorption bands.

To understand these observations it is useful to examine the calculated density of states for the B850 band. We show this in Figure 16, together with the absorption spectrum, for both the Q_y and the Q_x B850 bands. Couplings between Q_x BChls were calculated using the TDC method as described in ref 37. We found the intrapolypetide dimer coupling to be 117 cm^{-1} and the interpolypeptide dimer coupling to be 108 cm^{-1}. Next-to-nearest neighbor couplings are 7 cm^{-1} ($\alpha-\alpha$) and 3 cm^{-1} ($\beta-\beta$). We have then generated the B850 Q_x spectrum by shifting both E_α and E_β by 4340 cm^{-1} to the blue. This is comparable to the Q_x-Q_y energy difference for BChl in solution of 3740 cm^{-1}.[147] The BChl Q_x transition moments are all aligned, pointing from the cytoplasmic side of the membrane to the periplasmic side (i.e., away from the B800 ring). Owing to this orientation of the BChls, the Q_x ring oscillator strength is concentrated in the middle of the density of states, rather than near the red edge as it is for the Q_y band. Figure 16 reveals a particularly interesting picture of the energy funnel in LH2. The carotenoid $S_2 \leftarrow S_0$ transition lies at 550 nm, then we have the Q_x B850 density of states, then spanning the "hole" between this region and the B800/B850 Q_y region is the optically forbidden carotenoid $S_1 \leftarrow S_0$ transition.[148,149] Experiments on the B850-only LH2 complex suggest that there is B850 absorption in this 650−720 nm window, which probably accounts for the B670−B850 and B694−B850 energy transfer rates. This contribution to the spectral overlap, presumably arising from various intensity borrowing effects,[150−153] was not accounted for in our model. A final observation concerning the spectral funnel in LH2, is the somewhat striking observation that the only real "hole" in the B850 density of states lies at 800 nm (see also Figure 9); does this suggest another reason for having the B800 ring?

We conclude that investigation of the "B800"-B850 energy transfer time as a function of "B800"-B850 energy gap[145,146] or for example of position of the B850 band which may be shifted by site-directed mutagenesis,[49,154] provides many im-

portant insights into the energy transfer dynamics in LH2. However, owing to the broad and complex density of states of the B850 band, which in turn determines the B800−B850 spectral overlap, such studies, although systematic in conception, need careful analysis if quantitative information is to be obtained.

X. Concluding Remarks

Progress toward construction of a fully realistic description of the light harvesting processes has been hampered in the past by inaccurate knowledge of electronic couplings, electron−phonon coupling, and site energy distributions in antenna complexes. Recently, this information has become available, and we have been able to incorporate it into a detailed model for determining the ensemble average rate of energy transfer. Thus, we have been able to distinguish the roles played by line-broadening mechanisms that are due to fast fluctuations of the bath (electron−phonon coupling) from those that arise from the essentially static distribution of site energies (disorder). These line-broadening mechanisms both contribute to the ensemble average spectral overlap between donor emission and acceptor absorption, eq 7, as shown in Figure 6. The disorder has a significant effect on the calculated spectral overlap and energy transfer time, and our calculations have found it to influence profoundly the way we must model the B800 to B850 energy transfer dynamics (Table 1). Furthermore, the disorder is directly responsible for the moderate temperature dependence of the B800−B850 energy transfer rate (Figure 12). By examining "single molecule" calculations from within the ensemble average (Figure 5), the mechanism by which disorder broadens the B850 density of states (Figure 9) was elucidated. This spectral broadening of the density of acceptor states, in turn, affects the B800−B850 spectral overlap to a signifcant extent.

The theory, eq 8, can extrapolate smoothly between the extreme limits of localized acceptor through to delocalized acceptor states. It was found in the present study that the line-broadening mechanisms act in concert to define the "nature" of the B850 acceptor state, which is quasilocalized. Thus, the electronic scattering in the B850 band plays a role in promoting the energy transfer from B800 by increasing significantly the spectral cross section of the energy acceptor, as highlighted in Figures 9 and 10 and the associated discussion. This point was explored further in the calculations of the *Rps. acidophila* B800−B850 LH2 and reconstituted complexes; see section IX. These calculations of the B800−B850 energy transfer times were in close accord with trends in various experimental results, and the complex relationship between these energy transfer times and the precise overlap of the B800 emission band with the B850 density of states was revealed. In Figure 16, we depicted the large spectral window for the B850 energy acceptor, including both the Q_y and Q_x bands. It appears that the combination of fairly strongly coupled BChls together with the circular arrangement of the B850 BChls is advantageous to these organisms. The result is two broad spectral windows through which the B850 band can trap excitation directly and indirectly throughout an expanded spectral cross section.

It was reported that interaction of the B800 and B850 transition densities with the carotenoids has an effect on the B800−B850 electronic couplings (increasing them by approximately up to 30%), which in turn, leads to a faster calculated energy transfer time. This result suggests an indirect role played by the carotenoids in light-harvesting in LH2; through their involvement as bridging polarizable media.

In summary, we believe that the calculations reported in this work capture the essential details and principles of the light harvesting mechanism in LH2. The calculations of the energy transfer times reported in Tables 1 and 2 also reinforce the quantitative success of this model. In conclusion, we needed to include in our model detailed structural parameters, account of all the chromophores in the complex, accurate electronic couplings, electron−phonon couplings, disorder, and vibronic information. The B800−B850 spectral overlap and energy transfer rates had to be calculated as ensemble average quantities owing to the disorder in the BChl site energies. The picture of LH2 that emerges is of a complex system whose function cannot be readily predicted by examining its components individually. Instead, the true behavior emerges only after the whole system is included in the model. The interplay of electronic coupling and disorder allows construction of a robust system based on only two chemical species as chromophores to harvest radiation from most of the visible spectrum with near unit efficiency. Such a principle is likely to be a general aspect of photosynthetic energy transfer. For example, the mechanism and striking absence of temperature dependence of the accessory BChl (B) to special pair (P) energy transfer in the purple bacterial reaction center,[155−158] along with the remarkably rapid B to oxidized P energy transfer[159] very likely can be explained by a combination of electronic coupling over distances smaller than molecular sizes and its interplay with disorder.

Acknowledgment. This work was supported by the National Science Foundation and the Department of Energy. We wish to acknowledge I. R. Gould and B. P. Krueger for their contributions to Figure 13. R. J. Cogdell and J. L. Herek are thanked for discussions and communication of their unpublished work, and we gratefully acknowledge their generous provision of the B670-B850 absorption spectrum shown in Figure 16.

Appendix

A general framework for describing superexchange coupling for energy transfer has been reported previously.[67] It is based on generating effective donor and acceptor wave functions that include mixing with bridge configurations. Thus, the Hamiltonian for each of the donor and acceptor (denoted M) is written as $H = H_M + H_P + H'$ where the bridge (or "perturber") is labeled P, and H' is the interaction term which includes Coulombic interactions, spin−orbit terms, and charge transfer (CT) configurations (i.e., the possibility of significant overlap between the M and P wave functions). Hence, following Harcourt et al.[76] we write our molecule−perturber pair ground and excited-state wave functions as

$$\Phi^{00} = \phi_M^0 \, \phi_P^0 \tag{A1}$$

$$\Phi^{m0} = N(\phi_M^m \, \phi_P^0 + \lambda \phi_M^+ \, \phi_P^- + \mu \phi_M^- \, \phi_P^+ + \sum_p \eta_p \phi_M^0 \, \phi_P^p + ...) \tag{A2}$$

where Φ^{mp} denotes state m of the molecule and state p of the perturber, the λ, μ, and η are mixing coefficients described in the appendix, and N is the normalization constant that ensures $\langle \Phi^{m0} | \Phi^{m0} \rangle = 1$ ($N \approx 1$ for weak perturbations).

The orbital overlap-mediated superexchange interactions are thus promoted by interactions that, in a perturbation representation, would look like $D^*PA \rightarrow D^-P^+A \rightarrow DP^*A \rightarrow DP^+A^- \rightarrow DPA^*$, etc.[67] We have reported some molecular orbital calculations recently that suggest these type of interactions are particularly significant between the carotenoid and the B850 BChls in LH2.[61]

Owing to the intensity of the $S_2 \leftarrow S_0$ carotenoid transition and its energetic proximity to the BChl Q_y transition, it is likely

that Coulombic interactions play an important role, for example as described by Robinson,[140] who considered the intensity enhancement of electronic transitions by a proximate "perturber" molecule. It can be shown that the perturbations which we are interested in do not significantly affect the energy of the $\Phi^{m0} \leftarrow \Phi^{00}$ transition. However, the electronic transition density can be significantly perturbed, which in turn perturbs the matrix element for energy transfer from D to A. This is signaled by a perturbation of the dipole transition moment for the $m0 \leftarrow 00$ transition of the MP pair, eq 13.

$$\vec{\mu}_{m0;00} \approx \langle \Phi^{m0} | e\vec{r} | \Phi^{00} \rangle \tag{A3}$$

Monomer transition moments are indicated by superscripts M or P in eq 11. Approximate expression for these coefficients are given in eqs A4−A6:

$$\lambda \approx -\beta_{\mathrm{ET}}/A_{\mathrm{ET}} \tag{A4}$$

$$\mu \approx -\beta_{\mathrm{HT}}/A_{\mathrm{HT}} \tag{A5}$$

$$\eta_p \approx -\frac{V_{0p;m0}}{A_{0p;m0}} + \sum_{n,q} \frac{V_{0p;nq} V_{\mathrm{nq};m0}}{A_{0p;m0} A_{nq;m0}} \tag{A6}$$

where β_{ET} is the electron transfer matrix element between M and P, β_{HT} is the corresponding hole transfer matrix element, and A_{ET} and A_{HT} are the energy gaps between the charge-separated and locally excited configurations. The $V_{0p;m0}$, etc. are couplings between electronic excited states of the molecule and perturber, that are usually dominated by the Coulombic interaction (i.e., $V_{0p;m0} \approx V^{\mathrm{Coul}}$).

References and Notes

(1) McDermott, G.; Prince, S. M.; Freer, A. A.; Hawthornthwaite-Lawless, A. M.; Papiz, M. Z.; Cogdell, R. J.; Isaacs, N. W. *Nature* **1995**, *374*, 517.

(2) McDermott, G.; Prince, S. M.; Freer, A. A.; Isaacs, N. W.; Papiz, M. Z.; Hawthornthwaite-Lawless, A. M.; Cogdell, R. J. *Protein Eng.* **1995**, *8*, 43.

(3) Koepke, J.; Hu, X. C.; Muenke, C.; Schulten, K.; Michel, H. *Structure* **1996**, *4*, 581.

(4) Oling, F.; Boekema, E. J.; Dezarate, I. O.; Visschers, R.; van Grondelle, R.; Keegstra, W.; Brisson, A.; Picorel, R. *Biochim. Biophys. Acta* **1996**, *1273*, 44.

(5) Walz, T.; Jamieson, S. J.; Bowers, C. M.; Bullough, P. A.; Hunter, C. N. *J. Mol. Biol.* **1998**, *282*, 833.

(6) Cogdell, R. J.; Isaacs, N. W.; Freer, A. A.; Arrelano, J.; Howard, T. D.; Papiz, M. Z.; Hawthornthwaite-Lawless, A. M.; Prince, S. *Prog. Biophys. Mol. Biol.* **1998**, *70*, R1.

(7) Sundström, V.; Pullerits, T.; van Grondelle, R. *J. Phys. Chem. B* **1999**, *103*, 2327.

(8) Fleming, G. R.; van Grondelle, R. *Curr. Opin. Struct. Biol.* **1997**, *7*, 738.

(9) van Grondelle, R.; Monshouwer, R.; Valkunas, L. *Pure Appl. Chem.* **1997**, *69*, 1211.

(10) Freer, A.; Prince, S.; Sauer, K.; Papiz, M.; Hawthornthwaite-Lawless, A.; McDermott, G.; Cogdell, R.; Isaacs, N. W. *Structure* **1996**, *4*, 449.

(11) Jimenez, R.; Dikshit, S. N.; Bradforth, S. E.; Fleming, G. R. *J. Phys. Chem.* **1996**, *100*, 6825.

(12) Wu, H. M.; Savikhin, S.; Reddy, N. R. S.; Jankowiak, R.; Cogdell, R. J.; Struve, W. S.; Small, G. J. *J. Phys. Chem.* **1996**, *100*, 12022.

(13) Wu, H. M.; Ratsep, M.; Lee, I. J.; Cogdell, R. J.; Small, G. J. *J. Phys. Chem. B* **1997**, *101*, 7654.

(14) Sauer, K.; Cogdell, R. J.; Prince, S. M.; Freer, A.; Isaacs, N. W.; Scheer, H. *Photochem. Photobiol.* **1996**, *64*, 564.

(15) Alden, R. G.; Johnson, E.; Nagarajan, V.; Parson, W. W.; Law, C. J.; Cogdell, R. G. *J. Phys. Chem. B* **1997**, *101*, 4667.

(16) Nagarajan, V.; Johnson, E. T.; Williams, J. C.; Parson, W. W. *J. Phys. Chem. B* **1999**, *103*, 2297.

(17) Dracheva, T. V.; Novoderezhkin, V. I.; Razjivin, A. P. *Photochem. Photobiol.* **1997**, *66*, 605.

(18) Pullerits, T.; Hess, S.; Herek, J. L.; Sundström, V. *J. Phys. Chem. B* **1997**, *101*, 10560.

(19) Koolhaas, M. H. C.; Frese, R. N.; Fowler, G. J. S.; Bibby, T. S.; Georgakopoulou, S.; van der Zwan, G.; Hunter, C. N.; van Grondelle, R. *Biochemistry* **1998**, *37*, 4693.

(20) Koolhaas, M. H. C.; van der Zwan, G.; Frese, R. N.; van Grondelle, R. *J. Phys. Chem. B* **1997**, *101*, 7262.

(21) Vulto, S. I. E.; Kennis, J. T. M.; Streltsov, A. M.; Amesz, J.; Aartsma, T. J. *J. Phys. Chem. B* **1999**, *103*, 878.

(22) Zhao, Y.; Meier, T.; Zhang, W. M.; Chernyak, V.; Mukamel, S. *J. Phys. Chem. B* **1999**, *103*, 3954.

(23) Kumble, R.; Hochstrasser, R. M. *J. Chem. Phys.* **1998**, *109*, 855.

(24) Chachisvilis, M.; Kuhn, O.; Pullerits, T.; Sundström, V. *J. Phys. Chem. B* **1997**, *101*, 7275.

(25) Pullerits, T.; Sundström, V. *Acc. Chem. Res.* **1996**, *29*, 381.

(26) Pullerits, T.; Chachisvilis, M.; Sundström, V. *J. Phys. Chem.* **1996**, *100*, 10787.

(27) Hu, X. C.; Damjanovic, A.; Ritz, T.; Schulten, K. *Proc. Natl. Acad. Sci. U.S.A.* **1998**, *95*, 5935.

(28) Hu, X. C.; Ritz, T.; Damjanovic, A.; Schulten, K. *J. Phys. Chem. B* **1997**, *101*, 3854.

(29) Zhang, W. M.; Meier, T.; Chernyak, V.; Mukamel, S. *J. Chem. Phys.* **1998**, *108*, 7763.

(30) Zhang, W. M.; Meier, T.; Chernyak, V.; Mukamel, S. *Philos. Trans. R. Soc. (London) A* **1998**, *356*, 405.

(31) Kennis, J. T. M.; Streltsov, A. M.; Permentier, H.; Aartsma, T. J.; Amesz, J. *J. Phys. Chem. B* **1997**, *101*, 8369.

(32) Somsen, O. J. G.; Chernyak, V.; Frese, R. N.; van Grondelle, R.; Mukamel, S. *J. Phys. Chem. B* **1998**, *102*, 8893.

(33) Beekman, L. M. P.; Frese, R. N.; Fowler, G. J. S.; Picorel, R.; Cogdell, R. J.; van Stokkum, I. H. M.; Hunter, C. N.; van Grondelle, R. *J. Phys. Chem. B* **1997**, *101*, 7293.

(34) Monshouwer, R.; van Grondelle, R. *Biochim. Biophys. Acta* **1996**, *1275*, 70.

(35) Freiberg, A.; Timpmann, K.; Lin, S.; Woodbury, N. W. *J. Phys. Chem. B* **1998**, *102*, 10974.

(36) Scholes, G. D.; Gould, I. R.; Cogdell, R. J.; Fleming, G. R. *J. Phys. Chem. B* **1999**, *103*, 2543.

(37) (a) Krueger, B. P.; Scholes, G. D.; Fleming, G. R. *J. Phys. Chem. B* **1998**, *102*, 5378. (b) Krueger, B. P.; Scholes, G. D.; Fleming, G. R. *J. Phys. Chem. B* **1998**, *102*, 9603.

(38) Ray, J.; Makri, N. *J. Phys. Chem. A* **1999**, *103*, 9427.

(39) Krueger, B. P.; Scholes, G. D.; Gould, I. R.; Fleming, G. R. *Phys. Chem. Commun.* **1999**, *8*.

(40) van Grondelle, R.; Dekker, J. P.; Gillbro, T.; Sundström, V. *Biochim. Biophys. Acta* **1994**, *1187*, 1.

(41) Ma, Y. Z.; Cogdell, R. J.; Gillbro, T. *J. Phys. Chem. B* **1998**, *102*, 881.

(42) Ma, Y. Z.; Cogdell, R. J.; Gillbro, T. *J. Phys. Chem. B* **1997**, *101*, 1087.

(43) Hess, S.; Feldchtein, F.; Babin, A.; Nurgaleev, I.; Pullerits, T.; Sergeev, A.; Sundström, V. *Chem. Phys. Lett.* **1993**, *216*, 247.

(44) Shreve, A. P.; Trautman, J. K.; Frank, H. A.; Owens, T. G.; Albrecht, A. C. *Biophys. Biochim. Acta* **1991**, *1058*, 280.

(45) Monshouwer, R.; Dezarate, I. O.; van Mourik, F.; van Grondelle, R. *Chem. Phys. Lett.* **1995**, *246*, 341.

(46) Decaro, C.; Visschers, R. W.; van Grondelle, R.; Volker, S. *J. Phys. Chem.* **1994**, *98*, 10584.

(47) Fowler, G. J. S.; Hess, S.; Pullerits, T.; Sundstrom, V.; Hunter, C. N. *Biochemistry* **1997**, *36*, 11282.

(48) Hess, S.; Chachisvilis, M.; Timpmann, K.; Jones, M. R.; Fowler, G. J. S.; Hunter, C. N.; Sundstrom, V. *Proc. Natl. Acad. Sci. U.S.A.* **1995**, *92*, 12333.

(49) Hess, S.; Visscher, K. J.; Pullerits, T.; Sundström, V.; Fowler, G. J. S.; Hunter, C. N. *Biochemistry* **1994**, *33*, 8300.

(50) Kolaczkowski, S. V.; Hayes, J. M.; Small, G. J. *J. Phys. Chem.* **1994**, *98*, 13418.

(51) Joo, T. H.; Jia, Y. W.; Yu, J. Y.; Lang, M. J.; Fleming, G. R. *J. Chem. Phys.* **1996**, *104*, 6089.

(52) de Boeij, W. P.; Pshenichnikov, M. S.; Wiersma, D. A. *J. Phys. Chem.* **1996**, *100*, 11806.

(53) Nagasawa, Y.; Yu, J. Y.; Cho, M. H.; Fleming, G. R. *Faraday Discuss.* **1997**, 23.

(54) Fleming, G. R.; Cho, M. H. *Annu. Rev. Phys. Chem.* **1996**, *47*, 109.

(55) Yang, M.; Fleming, G. R. *J. Chem. Phys.* **1999**, *111*, 27.

(56) Cho, M. H.; Yu, J. Y.; Joo, T. H.; Nagasawa, Y.; Passino, S. A.; Fleming, G. R. *J. Phys. Chem.* **1996**, *100*, 11944.

(57) Förster, T. *Ann. Phys.* **1948**, *2*, 55.

(58) Förster, T. In *Modern Quantum Chemistry*; Sinanoglu, O., Ed.; Academic Press: New York, 1965; Vol. III, p 93.

(59) Lin, S. H. *Mol. Phys.* **1971**, *21*, 853.

(60) Scholes, G. D.; Harcourt, R. D.; Fleming, G. R. *J. Phys. Chem. B* **1997**, *101*, 7302.

(61) Scholes, G. D.; Gould, I. R.; Fleming, G. R. Unpublished.

(62) Nagae, H.; Kakitani, T.; Katoh, T.; Mimuro, M. *J. Chem. Phys.* **1993**, *98*, 8012.
(63) Scholes, G. D.; Ghiggino, K. P. *J. Phys. Chem.* **1994**, *98*, 4580.
(64) Scholes, G. D. In *Resonance Energy Transfer*; Andrews, D. L., Demidov, A. A., Eds.; Wiley: Chichester, 1999; p 212.
(65) McWeeny, R. *Methods of Molecular Quantum Mechanics*; Academic Press: London, 1992.
(66) Andrews, D. L. *Chem. Phys.* **1989**, *135*, 195.
(67) Scholes, G. D.; Harcourt, R. D. *J. Chem. Phys.* **1996**, *104*, 5054.
(68) Matos, J. M. O.; Roos, B. O.; Malmqvist, P.-A. *J. Chem. Phys.* **1987**, *86*, 1458.
(69) Dexter, D. L. *J. Chem. Phys.* **1953**, *21*, 836.
(70) Naqvi, K. R.; Steel, C. *Chem. Phys. Lett.* **1970**, *6*, 29.
(71) Choi, S.-I.; Jortner, J.; Rice, S. A.; Silbey, R. *J. Chem. Phys.* **1964**, *41*, 3294.
(72) Silbey, R.; Rice, S. A.; Jortner, J. *J. Chem. Phys.* **1965**, *43*, 3336.
(73) Koutecky, J.; Paldus, J. *Theor. Chim. Acta (Berlin)* **1963**, *1*, 268.
(74) Polák, R.; Paldus, J. *Theor. Chim. Acta (Berlin)* **1966**, *4*, 37.
(75) Azumi, T.; McGlynn, S. P. *J. Chem. Phys.* **1965**, *42*, 1675.
(76) Harcourt, R. D.; Scholes, G. D.; Ghiggino, K. P. *J. Chem. Phys.* **1994**, *101*, 10521.
(77) Scholes, G. D.; Harcourt, R. D.; Ghiggino, K. P. *J. Chem. Phys.* **1995**, *102*, 9574.
(78) Craig, D. P.; Thirunamachandran, T. *Molecular Quantum Electrodynamics*; Academic Press: New York, 1984.
(79) Prince, S. M.; Papiz, M. Z.; Freer, A. A.; McDermott, G.; Hawthornthwaite-Lawless, A. M.; Cogdell, R. J.; Isaacs, N. W. *J. Mol. Biol.* **1997**, *268*, 412.
(80) Dow, J. D. *Phys. Rev.* **1968**, *174*, 962.
(81) Scholes, G. D.; Ghiggino, K. P.; Oliver, A. M.; Paddon-Row, M. N. *J. Phys. Chem.* **1993**, *97*, 11871. (This experiment was also carried out in ethanol solvent, unpublished results.).
(82) Scholes, G. D.; Ghiggino, K. P.; Oliver, A. M.; Paddon-Row, M. N. *J. Am. Chem. Soc.* **1993**, *115*, 4345.
(83) Craig, D. P.; Thirunamachandran, T. *Chem. Phys.* **1989**, *135*, 37.
(84) Colson, S. D.; Robinson, G. W. *J. Chem. Phys.* **1968**, *48*, 2550.
(85) Juzeliunas, G.; Andrews, D. L. *Phys. Rev. B* **1994**, *49*, 8751.
(86) Juzeliunas, G.; Andrews, D. L. *Phys. Rev. B* **1994**, *50*, 13371.
(87) Andrews, D. L.; Juzeliunas, G. *J. Lumin.* **1994**, *60*−*61*, 834.
(88) Jimenez, R.; van Mourik, F.; Yu, J. Y.; Fleming, G. R. *J. Phys. Chem. B* **1997**, *101*, 7350.
(89) Yu, J. Y.; Nagasawa, Y.; van Grondelle, R.; Fleming, G. R. *Chem. Phys. Lett.* **1997**, *280*, 404.
(90) Krueger, B. P.; Scholes, G. D.; Yu, J. Y.; Fleming, G. R. *Acta Phys. Pol., A* **1999**, *95*, 63.
(91) Jordanides, X. J.; Lang, M. J.; Song, X.; Fleming, G. R. *J. Phys. Chem. B* **1999**, *103*, 7995.
(92) Gehlen, J. N.; Marchi, M.; Chandler, D. *Science* **1994**, *263*, 499.
(93) Schulten, K.; Tesch, M. *Chem. Phys.* **1991**, *158*, 421.
(94) Homoelle, B. J.; Edington, M. D.; Diffey, W. M.; Beck, W. F. *J. Phys. Chem. B* **1998**, *102*, 3044.
(95) Brooks, C. L.; Karplus, M.; Pettitt, B. M. *Proteins: A Theoretical Perspective of Dynamics, Structure, and Thermodynamics*; Wiley: New York, 1988.
(96) Fleming, G. R. *Proc. Natl. Acad. Sci. U.S.A.* **1998**, *95*, 15161.
(97) Reddy, N. R. S.; Small, G. J.; Seibert, M.; Picorel, R. *Chem. Phys. Lett.* **1991**, *181*, 391.
(98) Jean, J.; Chan, C.-K.; Fleming, G. R. *Isr. J. Chem.* **1988**, *28*, 169.
(99) Pullerits, T.; Freiberg, A. *Chem. Phys.* **1991**, *149*, 409.
(100) Beauregard, M.; Martin, I.; Holzwarth, A. R. *Biochim. Biophys. Acta* **1991**, *1060*, 271.
(101) Pullerits, T.; Freiberg, A. *Biophys. J.* **1992**, *63*, 879.
(102) Pullerits, T.; Visscher, K. J.; Hess, S.; Sundström, V.; Freiberg, A.; Timpmann, K.; van Grondelle, R. *Biophys. J.* **1994**, *66*, 236.
(103) Hess, S.; Åkesson, E.; Cogdell, R. J.; Pullerits, T.; Sundström, V. *Biophys. J.* **1995**, *69*, 2211.
(104) Mukamel, S. *Principles of nonlinear optical spectroscopy*; Oxford University Press: New York, 1995.
(105) Fleming, G. R.; Passino, S. A.; Nagasawa, Y. *Philos. Trans. R. Soc. (London) A* **1998**, *356*, 389.
(106) Simpson, W. T.; Peterson, D. L. *J. Chem. Phys.* **1957**, *26*, 588.
(107) Sumi, H. *J. Phys. Chem. B* **1999**, *103*, 252.
(108) Mukai, K.; Abe, S.; Sumi, H. *J. Phys. Chem. B* **1999**, *103*, 6096.
(109) Mukamel, S.; Rupasov, V. *Chem. Phys. Lett.* **1995**, *242*, 17.
(110) Gillie, J. K.; Small, G. J.; Golbeck, J. H. *J. Phys. Chem.* **1989**, *93*, 1620.
(111) Freiberg, A.; Godik, V. I.; Pullerits, T.; Timpmann, K. *Biochim. Biophys. Acta* **1989**, *973*, 93.
(112) Freiberg, A.; Godik, V. I.; Pullerits, T.; Timpmann, K. *Chem. Phys.* **1988**, *128*, 227.
(113) van Mourik, F.; Visscher, K. J.; Mulder, J. M.; van Grondelle, R. **1993**, *57*, 19.
(114) Lee, S.-Y.; Heller, E. J. *J. Chem. Phys.* **1979**, *71*, 4777.
(115) Myers, A. B. *J. Raman Spectrosc.* **1997**, *28*, 389.
(116) Myers, A. B. *Chem. Phys.* **1994**, *180*, 215.
(117) Li, B. L.; Johnson, A. E.; Mukamel, S.; Myers, A. B. *J. Am. Chem. Soc.* **1994**, *116*, 11039.
(118) Myers, A. B. *J. Opt. Soc. Am. B* **1990**, *7*, 1665.
(119) Fidder, H.; Knoester, J.; Wiersma, D. A. *J. Chem. Phys.* **1991**, *95*, 7880.
(120) Chernyak, V.; Mukamel, S. *J. Chem. Phys.* **1996**, *105*, 4565.
(121) Meier, T.; Chernyak, V.; Mukamel, S. *J. Chem. Phys.* **1997**, *107*, 8759.
(122) Onuchic, J. N.; Beraton, D. N.; Hopfield, J. J. *J. Phys. Chem.* **1986**, *90*, 3707.
(123) (a) van Oijen, A. M.; Ketelaars, M.; Köhler, J.; Aartsma, T. J.; Schmidt, J. *Science* **1999**, *285*, 400. (b) van Oijen, A. M.; Ketelaars, M.; Köhler, J.; Aartsma, T. J.; Schmidt, J. *Chem. Phys.* **1999**, *247*, 53.
(124) The $M(t)$ we have employed here is that reported for LH2 in ref 88. Our recent work suggests that the long exponential component is probably representative of complex-to-complex inhomogeneity.
(125) Renge, I.; Mauring, K.; Avarmaa, R. *J. Lumin.* **1987**, *37*, 207.
(126) Agarwal, R.; Xu, d.-H.; Fleming, G. R. Unpublished results.
(127) Knapp, E. W. *Chem. Phys.* **1984**, *85*, 73.
(128) Meier, T.; Chernyak, V.; Mukamel, S. *J. Phys. Chem. B* **1997**, *101*, 7332.
(129) Monshouwer, R.; Abrahamsson, M.; van Mourik, F.; van Grondelle, R. *J. Phys. Chem. B* **1997**, *101*, 7241.
(130) Chernyak, V.; Meier, T.; Tsiper, E.; Mukamel, S. *J. Phys. Chem. A* **1999**, *103*, 10294.
(131) Bakalis, L. D.; Knoester, J. *J. Phys. Chem. B* **1999**, *103*, 6620.
(132) Novoderezhkin, V.; Monshouwer, R.; van Grondelle, R. *J. Phys. Chem. B* **1999**, *103*, 10540.
(133) Closs, G. L.; Piotrowiak, P.; MacInnis, J. M.; Fleming, G. R. *J. Am. Chem. Soc.* **1988**, *110*, 2652.
(134) Closs, G. L.; Johnson, M. D.; Miller, J. R.; Piotrowiak, P. *J. Am. Chem. Soc.* **1989**, *111*, 3751.
(135) Kroon, J.; Oliver, A. M.; Paddon-Row, M. N.; Verhoeven, J. W. *J. Am. Chem. Soc.* **1990**, *112*, 4868.
(136) Kilså, K.; Kajanus, J.; Mårtensson, J.; Albinsson, B. *J. Phys. Chem. B* **1999**, *103*, 7329.
(137) Scholes, G. D.; Ghiggino, K. P. *J. Chem. Phys.* **1995**, *103*, 8873.
(138) Lin, S. H.; Xiao, W. Z.; Dietz, W. *Phys. Rev. E* **1993**, *47*, 3698.
(139) Ratner, M. A. *J. Phys. Chem.* **1990**, *94*, 4877.
(140) Robinson, G. W. *J. Chem. Phys.* **1967**, *46*, 572.
(141) Scholes, G. D. *J. Phys. Chem.* **1996**, *100*, 18731.
(142) Scholes, G. D.; Turner, G. O.; Ghiggino, K. P.; Paddon-Row, M. N.; Piet, J. J.; Schuddeboom, W.; Warman, J. M. *Chem. Phys. Lett.* **1998**, *292*, 601.
(143) Bandilla, M.; Ucker, B.; Ram, M.; Simonin, I.; Gelhaye, E.; McDermott, G.; Cogdell, R. J.; Scheer, H. *Biochim. Biophys. Acta* **1998**, *1364*, 390.
(144) Fraser, N. J.; Dominy, P. J.; Ücker, B.; Simonin, I.; Scheer, H.; Cogdell, R. J. *Biochemistry* **1999**, *38*, 9684.
(145) Leupold, D.; Stiel, H.; Ehlert, J.; Nowak, F.; Teuchner, K.; Voigt, B.; Bandilla, M.; Ücker, B.; Scheer, H. *Chem. Phys. Lett.* **1999**, *301*, 537.
(146) Herek, J. L.; Fraser, N. J.; Pullerits, T.; Martinsson, P.; Polívka, T.; Yartsev, A.; Scheer, H.; Cogdell, R. J.; Sundström, V. Submiited.
(147) Bellacchio, E.; Sauer, K. *J. Phys. Chem. B* **1999**, *103*, 2279.
(148) Polívka, T.; Herek, J. L.; Zigmantas, D.; Akerlund, H. E.; Sundström, V. *Proc. Natl. Acad. Sci. U.S.A.* **1999**, *96*, 4914.
(149) Krueger, B. P.; Yom, J.; Walla, P. J.; Fleming, G. R. *Chem. Phys. Lett.* **1999**, *310*, 57.
(150) Fischer, G. *Vibronic Coupling: The Interaction between the Electronic and Nuclear Motions*; Academic Press: London, 1984.
(151) Langhoff, C. A.; Robinson, G. W. *Mol. Phys.* **1975**, *29*, 613.
(152) Robinson, G. W.; Berg, J. O. *Can. J. Phys.* **1975**, *53*, 2068.
(153) Chock, D. P.; Jortner, J.; Rice, S. A. *J. Chem. Phys.* **1968**, *49*, 610.
(154) Fowler, G. J. S.; Visschers, R. W.; Grief, G. G.; van Grondelle, R.; Hunter, C. N. *Nature* **1992**, *355*, 848.
(155) Haran, G.; Wynne, K.; Moser, C. C.; Dutton, P. L.; Hochstrasser, R. M. *J. Phys. Chem.* **1996**, *100*, 5562.
(156) Jonas, D. M.; Lang, M. J.; Nagasawa, Y.; Joo, T.; Fleming, G. R. *J. Phys. Chem.* **1996**, *100*, 12660.
(157) Stanley, R. J.; King, B.; Boxer, S. G. *J. Phys. Chem. B* **1996**, *100*, 12052.
(158) Arnett, D. C.; Moser, C. C.; Dutton, P. L.; Scherer, N. F. *J. Phys. Chem. B* **1999**, *103*, 2014. van Brederode, M. E.; van Mourik, F.; van Stokkum, I. H. M.; Jones, M. R.; van Grondelle, R. *Proc. Natl. Acad. Sci. U.S.A.* **1996**, *96*, 2054.
(159) Jackson, J. A.; Lin, S.; Taguchi, A. K. W.; Williams, J. C.; Allen, J. P.; Woodbury, N. W. *J. Phys. Chem. B* **1997**, *101*, 5747.